ECOLE

POLYTECHNIQUE

IN2P3-CNRS

CMS-TN/94-152, IHEP 94-31, INR-984/94, X-LPNHE 94-01

NEW TESTBEAM RESULTS OF SHASHLIK AND PRESHOWER PROTOTYPES

J. Badier[1], S. Bityukov[2], P. Bordalo[3], Ph. Busson[1], C. Charlot[1], L. Dobrzynski[1], I. Golutvin[5], E. Guschin[4], I. Ivanchenko[5], V. Lapshin[2], V. Marin[4], P. Moissenz[5], Y. Musienko[4], V. Obraztsov[2], A. Ostankov[2], V. Popov[3], S. Ramos[3], G. Roullet[6], C. Seez[7], S. Sergueev[5], I. Semenyuk[4], V. Soushkov[2], R. Tanaka[1], J-C. Vanel[1], J. Varela[3], T.S. Virdee[7], A. Zaitchenko[2], N. Zamiatin[5]

March 21, 1994

[1]LPNHE-Ecole Polytechnique, IN2P3-CNRS, Palaiseau, France
[2]IHEP, Protvino, Russia
[3]LIP, Lisbon, Portugal
[4]INR, Moscow, Russia
[5]JINR, Dubna, Russia
[6]DAPNIA-Service de Physique des particules, Saclay, France
[7]Imperial College, London, UK

Contents

List of Tables

List of Figures

1 Introduction

Electromagnetic calorimeters will be essential tools at future LHC experiments since their precision improves with increasing energies. Among the performances to be achieved by the electromagnetic calorimeter are good hermeticity, radiation hardness and high speed. The most stringent requirement concerning energy resolution comes from the ability to detect an intermediate mass Higgs boson decaying into two gammas. This will require a very good energy resolution, angular resolution and π^0 rejection capability [1]. The electromagnetic calorimeter is also required to have a wide dynamical range up to few TeV, with good linearity. Finally, it should match the stringent constraints from mechanical construction and cost.

The use of lead-scintillator sandwich type calorimeter readout by WLS fibres has been suggested since mid-1980's [2]. Such shashlik calorimeter [3] has been proposed as the baseline choice for electromagnetic calorimetry in the CMS experiment [4, 5]. It should satisfy the quoted above requirements concerning energy resolution. It allows for very good hermeticity and compactness. It can match the 25ns bunch crossing time and can be readout in the 4T solenoidal magnetic field of CMS. If combined with a silicon strip detector, it would allow for sufficient π^0 rejection and photon direction measurement.

The purpose of this note is to present the results of measured performances of small shashlik prototypes tested in conjunction with a small silicon strip preshower prototype.

2 Experimental setup

Two matrices of calorimeter towers were exposed and tested in the H2 beam line at CERN SPS. One is a 3×3 matrix (nonet) of non projective towers already tested in 1992 [6]. The other is a 4×3 matrix of projective towers. In front of these prototypes, two layers of silicon strips were installed as indicated in Fig. 1.

2.1 The detectors

2.1.1 The shashlik prototypes

Each calorimeter tower consists of a set of identical layers of lead and scintillator tiles of 2mm and 4mm respective thickness. The scintillator tiles, manufactured at IHEP using casting technology, are optically isolated by two sheets of white paper of about 100 μm thickness.

The WLS fibres of 1.2 mm diameter are running perpendicular to the tiles through holes. We used Y7 type of WLS produced by Kuraray for the nonet, while the projective tower prototype was equipped with K27 fibres produced at INR (Moscow). These fibres are made out of polystyrene with a fluorinated PMMA cladding. The core contains scintillating dopants whose absorption spectrum is well matched with the emission spectrum of the para-terphenyl + POPOP scintillator. The resulting emission spectrum peaks at $\lambda_{max} = 500$ nm (530 nm) for Y7 (K27) fibres.

Each tower of the nonet prototype has a parallelepipedical shape of $47 \times 47 \times 440$ mm^3 dimensions. Each tile has 25 holes of 1.3 mm diameter arranged in a 5×5 matrix. The

	Non projective	Projective
Tower lateral size	47×47 mm^2	52×52 mm^2 (front) 64×64 mm^2 (rear)
Number of layers	72	75
Scintillator / lead	4 mm / 2 mm	
Total length	26X0	27X0
Radiation length	17 mm	
Moliere radius	34 mm	
Density	4.5 g/cm^3	
Scintillator	polytstyrene + 0.5 % POPOP + 2 % para-terphenyl	
WLS fibre	Y7, ϕ 1.2 mm	K27, ϕ 1.2 mm
Number of fibres	25	36
Interfibre distance	9.5 mm	
Readout	photodiode + preamplifier	photomultiplier

Table 1: Shashlik prototypes parameters

interfiber distance is 9.5 mm and the distance from the outermost fibre to the edge of the tower is 4.7 mm. The WLS fibres were aluminized by sputtering at the front face of the tower. At the rear end, the fibres were bundled and coupled through an hexagonal plexiglas light mixing guide to a 10 × 10 mm^2 silicon PIN photodiode. Each photodiode (Hammamatsu S3590, 500μ thickness) was followed by a low noise charge amplifier built at INR [7]. The measured equivalent noise charge with the photodiode capacitance of 30pF and with the shaping time of 20 ns (RC-CR shaping) was measured to be 900e^- [7, 8]. More details on the mechanical construction and readout of these towers can be found in [6].

The projective towers have a truncated pyramidal shape as shown in Fig. 1. The front face size is 52 × 52 mm^2 and the rear face size is 64 × 64 mm^2. Instead of aluminization, each fibre is looped at the front face and fed back through the tower to a photomultiplier (XP2961, 8 stages, green extended photocathode) at the rear side. Such U-shape loops act as practically ideal mirrors (reflectivity > 95%) and offer the advantage of reducing potential non-uniformity in light collection. The WLS fibres are parallel from each other in a 6 × 6 matrix as in the non-projective prototype, and hence the distance between the outermost fibre and the scintillator edge is increasing with increasing depth. The shashlik prototypes parameters are summarized in Table 1.

The preamplifier (nonet) and the photomultiplier (projective prototype) outputs were connected by a 90m long coaxial cable to postamplifiers (Fig. 2). Additional Lecroy amplifiers with adjustable gain were used to put the signal into the ADC range (12 bits charge sensitive Lecroy 2282A). No attempt was made to unfold the cable effect on the signal. The data were taken with a gate duration of 160 ns. To increase the precision of the measurements on the full dynamic range (from few 10 MeV to 200 GeV) we have split the signal of each channel and made use of two different gain amplifiers with a gain

ratio of 10.

2.1.2 The preshower prototype

The preshower detector consists of two layers of 29 silicon strips with 2mm pitch distance. The first plane is preceded by a $2X_0$ copper absorber. The two planes are separated by a $1X_0$ length additionnal copper absorber, as indicated in Fig. 1. The strip axis of the second plane is perpendicular to the one of the first plane to allow for both transverse coordinate measurements. These detectors were manufactured by ELMA (Moscow) from 3.6 kΩ.cm n-type FZ-Wacker silicon. The size of the silicon plate is 60×60 mm^2 and the wafer width is $400\mu m$. The strip area is 1.2 cm^2 with a capacitance of 27 pF.cm^{-2}. The full depletion is obtained at the reverse bias of 170V.

The readout was performed by the AMPLEX card used in LEP experiments [9]. The measured energy was calibrated by normalizing the signal in the two planes plus the shashlik one to the incident beam energy.

2.2 The beam line

The measurements were performed in the H2 beam line of the CERN SPS. The calorimeter towers were mounted on a platform which allows for horizontal and vertical translations with respect to the beam line. The platform position was measured in rod counts with one count being equal to 1.05 mm. The projective towers were aligned such that the beam line was along the intersection of the horizontal and vertical median planes of the setup (see Fig. 1). The platform also allows for rotation of the calorimeter prototypes around the vertical axis, so that particles could be sent at a chosen angle θ_z (limited to few degrees) with respect to the fibre axis.

Upstream of the calorimeter, a set of five scintillator counters was used to define the trigger (see Fig. 3). The requirement of a 5-fold coincidence $S1 \times S2 \times S3 \times \times S4 \times S5$ defines the so called narrow beam, whose section is limited by the two smaller counters S4 and S5 to about 5×5 mm^2. We also used the so called wide beam defined by $S1 \times S2 \times S3$ coincidence whose typical section is 20×20 mm^2.

The beam coordinates were measured by a set of three delay wire chambers, U1,U2 and U3, of 10×10 cm^2 active area, the last being at a distance of 74 cm from the prototype front face. The coordinate resolution of each chamber was measured to be $250\mu m$.

Beams of 10,15,20,40,80,120 and 150 GeV e^- were sent into the detectors at small angles θ_z with respect to the fibre axis. The beam rate was about 5000-10000 $S1 \times S2 \times S3$ per spill of 2.6 sec duration every 14 sec, leading to about 300 events on tape per spill. Muon beams of 225 GeV were also used to calibrate the preshower detector and to measure the muon response in the shashlik and preshower prototypes.

3 Experimental data and method

The results presented in this note were obtained by analysing the following sets of data samples (the exhaustive list of data recorded in summer 93 can be found in appendix 1):

- may 93 runs
  - *projective* prototype *calibration*, 40 GeV, narrow beam, about 10000 events per run
  - *projective* prototype *horizontal scan 1*, X=731.5-813.5, Y=873, 40 GeV, wide beam, about 5000 events per run
  - *projective* prototype *vertical scan*, X=780.5, Y=831-915, 40 GeV, wide beam, about 5000 events per run
  - *projective* prototype *horizontal scan 2*, X=731.5-820.5, Y=878, 40 GeV, wide beam, about 5000 events per run
  - *projective* prototype with *preshower energy scan*, 10,15,20,40,80,120,150 GeV, narrow beam, about 10000 events per run
  - *projective* prototype with *preshower uniformity scan in T7*, 40 GeV, wide beam, about 5000 events per run
- august 93 runs
  - *nonet calibration*, 40 GeV, narrow beam, about 5000 events per run
  - *nonet energy scan* at $\theta_z = 0$ *degree*, 15,20,40,80,120,150 GeV, narrow beam, about 5000 events per run
  - *nonet energy scan* at $\theta_z = 3$ *degrees*, 15,20,40,80,120,150 GeV, narrow beam, about 5000 events per run
  - *nonet* with *preshower energy scan* at $\theta_z = 0$ *degree*, 15,20,40,80,120,150 GeV, narrow beam, about 10000 events per run
  - *preshower calibration* run, 225 GeV μ, about 10000 events per run
  - *projective* prototype *calibration*, 40 GeV, narrow beam, about 5000 events per run
  - *projective* prototype *energy scan* at $\theta_z = 0$ *degree*, 10,15,20,40,80,120,150 GeV, narrow beam, about 5000 events per run
  - *projective* prototype *energy scan* at $\theta_z = 3$ *degrees*, 10,15,20,40,80,120,150 GeV, narrow beam, about 5000 events per run

Beam coordinates were obtained from chambers by the time differences of the signal measured by TDCs, $t_{left} - t_{right}$ or $t_{up} - t_{down}$. These values are converted in mm after calibration of the chambers by sending reference signals at the middle (0 mm) and at ± 30 mm in each chambers. Cuts on TDC sum (whose value is constrained by the delay line lenght) for each coordinate measurement allows for double hit removal as illustrated in Fig. 4. Final U1 profile for narrow (wide) beam is shown in Fig.5 (Fig.6). The beam position was obtained from the fit of the three chambers measurements and extrapolated to the front face of the prototypes. This procedure leads to an impact point resolution of less than 300μ with an efficiency of about 60% (efficient track is a track with hit in all chambers and good χ^2 from the fit of both x and y coordinates).

Pedestal runs were taken every 10 runs using a trigger gate starting randomly out of the spill duration. The towers were calibrated with 40 GeV electrons. About 3000-5000 e^- taken with narrow beam were sent in the central region of the central tower at normal incidence. The procedure was repeated for the other towers by translating the platform in x and y according to the transverse size of the towers. For the projective ones, the translation was based on the front face size. On average, 83% (88%) of the total incident energy was deposited in the tower under calibration for the nonet (projective) prototype.

In the results presented below, the pedestal values have been subtracted without zero suppression to avoid any bias in the energy sum distributions. All the data have been calibrated offline, with a statistical precision of 0.2%. However, due to systematical effects as local non uniformities and table position uncertainties, the tower to tower intercalibration is $\leq 1\%$. In particular, the translation step adopted for the projective towers and the small angle between tower axis and beam due to the projectivity leads to systematical errors for asymmetry calculations. This however have a small effect on the final energy resolution due to the relative amount of energy deposited in the central tower to the neighbors.

The data were selected to have an efficient track reconstruction from beam chambers as previously defined. The electron beams were very clean so that no offline treatment was applied to remove any contamination from charged hadrons. In calculating the energy sum deposited in the calorimeter, we have used the low gain and high gain information of each tower in the following way: for each event, high gain was selected if not being close to saturation, that is if the low gain value was lower than 80 picocoulombs.

4 Experimental results

4.1 Linearity

The energy responses of the shashlik nonet and projective prototypes are shown in Fig. 7 as a function of the beam energy. The points are normalized to the value obtained at 80 GeV. The errors are dominated by systematic beam energy uncertainties due to magnet effects. The projective prototype response is found to be linear within $\pm 1\%$ while the nonet one presents deviation from linearity up to 5% at low energies. Apart from possible electronic nonlinearity, one can expect two sources of nonlinearity in such calorimeters. Firstly, the finite attenuation length of the WLS fibres leads to non linearity since the shower average depth depends on energy. The observed effect can be qualitatively reproduced by taking the approximate value of $\lambda_{att} = 100$ cm. Such an effect should be enforced in the nonet case due to non perfect light reflection at the aluminized end of the towers. Another effect should appear in case of projective towers since, as previously mentioned, the fibres being parallel to each other, the distance from the edge to the outermost fibre is increasing linearly with depth. The fact that no linearity deviation is observed with projective towers indicates that such light collection effects are small or cancelling each other and that the non linearity observed with the nonet is presumably due to electronic. In the data presented below, no attempt has been made to correct for this non linearity effect at low energies.

4.2 Energy resolution

4.2.1 Energy resolution for the nonet

The energy distribution for 40 Gev e^- is presented in Fig. 8. The fitted relative resolution is $\frac{\sigma}{E} = 2.0\%$. One can also notice some events which present an excess in the measured energy. This effect is unforced at 150 GeV as shown in Fig. 9. Such tail has been identified as resulting from the shower leaking particles at the rear of the towers and giving signal by hitting the silicon photodiode (see section 4.5). When limiting the fit to the gaussian part of the distribution, one finds a resolution of $\frac{\sigma}{E} = 1.1\%$ at 150 GeV.

The Fig. 10 presents the energy distribution obtained when sending the particle at $\theta_z = 3$ degrees, and compared to the previous one. We observe a small increase in the mean energy due to the increase in shower containment. Consequently, the amount of high energy tail in the distribution is decreased. The observed width of the distribution is clearly larger due to the change in impact point which for $\theta_z = 3$ degrees was at few millimeters from the tower edge.

The energy resolution of the nonet prototype at normal incidence is shown in Fig. 11 as a function of the beam energy. The energy resolution can be well parametrized by

$$\frac{\sigma_E}{E} = \frac{a}{E} \oplus \frac{b}{\sqrt{E}} \oplus c$$

with

$$a = 460 \pm 6\ MeV$$

$$b = 0.089 \pm 0.005\ GeV^{\frac{1}{2}}$$

$$c = 0.8 \pm 0.1\%$$

On the results presented on Fig. 11, the electronic noise has been subtracted. The quoted errors are largely dominated by systematics. These results are in agreement with previous measurements on the nonet prototypes [6] concerning the stochastic and the constant terms.

The measured electronic noise corresponds to $160MeV$ per channel on 8 channels (summation occurs on only 8 channels due to a very noisy ninth channel). It has been measured from the pedestal runs and has been checked to be in agreement with the fitted value. This value is slightly worse than the previously measured noise of $350MeV$ [6] on 9 channels which was in good agreement with the expected noise per channel resulting from the chosen shaping time of 20ns and the photodiode capacitance of 30 pF.

4.2.2 Energy resolution of projective prototype

Fig. 12 presents the energy distribution as measured by the prototype with projective towers for 40 GeV electrons. The shape is well described by a gaussian fit leading to a relative resolution of $\frac{\sigma_E}{E} = 1.9\%$ in relative agreement with the measured value for the nonet. At 150 GeV incident energy (Fig. 13), the resolution is found equal to 1.1%, as for the nonet. Now the high energy tail observed with the nonet does not exist since the projective towers were readout by photomultipliers.

The energy resolution as a function of the beam energy is presented on Fig. 14. The energy summation runs for 9 towers. The corresponding correlated noise of 169 $\pm$ 2 MeV has been subtracted in the presented data. We have checked that this value is consistent with a three parameter fit including a noise term. To check for possible effect of local non uniformity, the energy resolution has been obtained by studying the energy distribution in bins of transversal beam size of 1.5 $\times$ 1.5 mm^2. The result presented in Fig. 14 corresponds to the central bin. The fit results for each bin are presented in Fig. 15. The result is

$$\frac{\sigma_E}{E} = \frac{b}{\sqrt{E}} \oplus c$$

with

$$b = 0.096 \pm 0.008 \; GeV^{\frac{1}{2}}$$

$$c = 0.9 \pm 0.1\%$$

One can notice the correlation between the fitted values of the stochastic and constant terms. The above given values correspond to the average of the results in each bin and the errors are taken as the RMS of the distribution. One found a slightly increased but compatible value for the stochastic term, when compared to the nonet result. The constant term is in agreement with the one found for the nonet.

Such a constant term may arise from several reasons: energy longitudinal and lateral leakage; intercalibration errors; mechanical construction and assembling of towers. The intercalibration errors has been found to be negligible. The energy leakage, estimated from Monte Carlo calculations amounts to 2.8% at 150 GeV with relative fluctuation of 0.2% (see section 5). The remaining effect is likely to come from the modest quality of the mecanical construction of both nonet and projective towers prototypes. A detailed investigation of gap and light collection effects is reported in section 5.

4.2.3 Energy resolution with preshower

The energy distribution for the shashlik nonet with passive preshower in front is shown in Fig. 16 and compared with the one obtained without the preshower, for 150 GeV e^-. The energy response of the two preshower layers are presented in Fig. 17. The preshower response has been calibrated by normalizing the shashlik plus preshower response to the beam energy. The energy resolution of the combined shashlik and preshower calorimeter has been obtained by minimizing the width of the weighted sum

$$E = \alpha E_{PS1} + \beta E_{PS2} + \gamma E_{NON} + E_0$$

where E_{PS1}, E_{PS2} and E_{NON} are respectively the measured energies in preshower plane 1, in preshower plane 2 and in shashlik nonet. The term E_0 is introduced to account for the energy loss in the first absorber before the shower starts to develop. The resulting resolution is shown in Fig. 11 together with the result of a quadratic fit, and compared with the result obtained for the nonet only. The result obtained after noise subtraction is

$$\frac{\sigma_E}{E} = \frac{b}{\sqrt{E}} \oplus c$$

with

$$b = 0.100 \pm 0.005\ GeV^{\frac{1}{2}}$$

$$c = 0.8 \pm 0.1\%$$

One can observe that the points obtained with the preshower are systematically higher than without the preshower, which leads to the significant increase of the stochastic term. The degradation of the energy resolution due to the preshower can be parametrized by $\frac{4.6\%}{\sqrt{E}}$. However, such an increase is not expected from Monte Carlo simulations (see Fig. 38) due to the low level of energy dissipated in the preshower planes. The reason of such a discrepancy is presumably due to bad working conditions of the first plane during these tests resulting in a loss of information on the shower development.

4.3 Lateral uniformity of the response

A particular attention in these tests has been payed to the study of the uniformity of the response of the shashlik prototypes since light collection is known to introduce non-uniformity in such lead-scintillator sandwich type calorimeter. In addition to the potential source of non-uniformity coming from the light reflection on the edges of the scintillator tiles, the wavelength shifting fibres also affect the uniformity of the light collection. As reported in section 5.4, Monte Carlo simulations predict on overall effect limited to 2-3 % light yield variation from one tower edge to the other, although this value is found to be strongly dependent on the optical parameters (see section 5.4). Another expected effect for the projective towers is a light yield drop at the edge of the tower do to the variable distance between the outermost fibre and the edge. Finally, one is interested to study the influence of the preshower on these effects.

4.3.1 Uniformity of the response for projective towers

The mean energy response of the projective prototype as a function of the horizontal coordinate for 40 GeV e^- is shown in Fig. 18. In this scan, the vertical beam position is centered on the central fibre line. Horizontal coordinate is plotted in table counts units. The range cover the full size of the central tower (tower number 7) from one edge to the other. We observe a strong non uniformity of the response of about 6% amplitude. When parametrizing the observed position dependence, one can recover a uniformity within $\pm 1\%$. The residual non-uniformity is clearly correlated with fibres positions near which we observe an increase of signal as expected from light collection simulations. The distribution of the mean energy values (lower plot in Fig. 18) presents a width of $\sigma = 0.51\%$.

The same plots for the horizontal scan between two layers of fibres are presented in Fig. 19. For this scan, the data have been corrected offline for a too high rate in data taking leading to an increase of photomultipliers gains. The beam profile was large enough so that the two scans partly overlap from each other. We corrected the data from this scan by asking an equal response as for the previous scan for particle hitting the tower at the same point. The observed variation of the mean energy as a function of the x position is analog to the one from previous scan, except for the residual non-uniformity

after the fit which does not present any more the small oscillations due to the fibres. The resulting spread of the mean energy distribution is therefore lowered to $\sigma = 0.40\%$.

The result from the horizontal scan across fibres is also shown in Fig. 20 extending now from the center of tower 6 to center of tower 8. One can clearly see the effect of the projective crack (x = -31.0 mm) for which the response is decreased by 15% with respect to the value at tower center. The size of the crack is of the order of $\pm$1mm (FWHM) in agreement with what is expected from mecanical construction and tower alignment precision on the platform. The other crack (x = +24 mm) tilted by an angle of 1.7 degree due to projectivity presents a clearly different behavior with a signal decrease of only 7% with respect to the signal at the center. The size of the tower estimated from the crack positions is 55.0 $\pm$ 0.9 mm in relative agreement with the expected 56.4 mm size at shower average, taking 10 X_0 as average shower length at 40 GeV. The energy resolution is presented in Fig. 21 for beam impact at tower center and in the tilted crack. The relative resolution is worse by 30% when shooting in the tilted crack. For a beam impact along the projective crack, the energy resolution is found to be 4.2% compared to 1.7% at tower center.

4.3.2 Uniformity of the response with preshower

In Fig. 22 (Fig. 23) are presented the mean energy measured in the projective prototype with the preshower in front as a function of x coordinate (y coordinate) for several y (x) positions. In particular the x scan at the same y position (y=-7.5 mm) as for the x scan across fibres without preshower shows a slightly lower non-uniformity of $\sim$ 4%. The most central x scan (y = +3 mm) presents a uniformity even better than $\pm$2% without any corrections. This may indicates that the non uniformity coming from light collection is very quickly smeared by the transversal extension of the shower, so that the $3X_0$ from the preshower are sufficient to slightly decrease the non uniformity effect. One also notice in Fig. 22,23 that the amplitude of the non-uniformity increases when going toward the tower edges. Finally, no degradation of the energy resolution is observed when shooting in the tilted crack with the preshower in front as can be seen in Fig. 21.

4.3.3 Global self corrections of non uniformities

When presenting the results of the horizontal scans, we have shown a correction based on a empirical parametrization of the measured position dependence of the response. Such a correction would need a very precise knowledge of the track impact and angle, only possible to achieve for charged particles from central tracker and preshower measurements. A self correction using only the calorimeter information should be preferred. This can be achieved by using the measured asymmetry as an estimate of the position inside the tower and applying an asymmetry dependent correction on the measured energy. The measured energy as a function of the horizontal asymmetry is plotted in Fig. 24. In this plot the absolute value of the asymmetry has been taken in order to search for a symmetric correction with respect to the tower center. Hence, we have ignored the differences of the energy response near the projective and the tilted crack so that the correction function has been extracted from a fit of the mean absolute value of the asymmetry up to 0.3 which corresponds to the beginning of the cracks (see Fig. 25). The result of such

a correction is presented in Fig. 26. We obtain a uniformity of the response at the level of $\pm 1\%$ over the full tower size except in the crack region where no correction has been applied. The remaining question is to know wether such correction can be applied globally on all towers of the final calorimeter or whether one has to tabulate such correction for each tower. Since the effect is due to light collection, there is some hope that if the optical parameters of the tiles are well controlled, a unique global correction could be applied. To check this hypothesis, in producing Fig. 26, the same correction taken from tower number 7 has been applied to half of the tower 6 response (left of the projective crack). Hence, one can see that global correction seems to work well, at least for two towers.

One can further improve the method by taking the ratio of the central row sum to the upper and lower rows sum instead of the energy sum. Such ratio offers the advantage of being independent of the shower energy in first approximation, since the shower transversal profile does very weakly depend on energy. As shown in Fig. 27, the non-uniformity which is visible for the central row sum has been smoothed in the sum of upper and lower rows because the energy comes from the shower tail. Hence, the proposed ratio follows closely the non-uniformity of the total sum, as shown in Fig. 27. The non-uniformity and resolution after a correction based on this ratio are shown in Fig. 28. The resulting non-uniformity is limited to $\pm 1\%$ in the central region. In this method, the width of the correlation between the proposed ratio and asymmetry is bigger than when taking the energy sum, due to fluctuations in the energy measurement in the neighboring towers. It is however compensated for by the fact that one can use the entire electron spectrum to define the correction function in this case.

4.4 Position and angular resolution

Position resolution of the shashlik nonet and projective prototypes have been investigated as a function of the shower energy and position. The method is based on an asymmetry measurement (see [10]). The asymmetry is defined by

$$A(x) = \frac{\sum_j E_{imax-1} - \sum_j E_{imax+1}}{E_{tot}}$$

where i denotes the tower index along the axis corresponding to the coordinate to be measured, j the tower index along the orthogonal axis. For the nonet with the photodiode readout, a better estimate is obtained by taking only the towers with index $j = jmax$ instead of the sum, in order to limit the effect of the electronic noise. The Fig. 29 presents the usual S-shape of the asymmetry vs beam position which has been unfolded in the following way. The mean asymmetry is fitted locally (within $\pm$ 2mm) by a linear curve as a function of the position to provide the estimate $\hat{x}$ of the position. The position resolution is then obtained as the width of the distribution of

$$\hat{x} - x_{beam}$$

where x_{beam} stands for the beam position.

4.4.1 Position resolution for the nonet

The nonet position resolution as a function of incident energy is presented in Fig. 30 for $\theta_z = 0$ and 3 degrees incident angles and at the center of the central tower. In the presented data, three measurements that are x position from the energy scan at $\theta_z = 0$, y position at $\theta_z = 0$ and y position at $\theta_z = 3$ degrees (the θ_z angle does not affect y measurement) have been combined and used to estimate the systematic uncertainties in the position resolution determination. These systematical errors are included in the presented data. The data are fitted with the quadratic function

$$\sigma_{x,y} = \frac{a}{E} \oplus \frac{b}{\sqrt{E}} \oplus c$$

At 0 degree angle, no significative constant term is found so that the last parameter has been fixed to 0. One gets:

$$a = 37.3 \pm 2.6 \; mm.GeV$$

$$b = 9.3 \pm 0.4 \; mm.GeV^{\frac{1}{2}}$$

It corresponds to 1.7 mm at 40 GeV and 0.8 mm at 150 GeV. At 3 degrees angle, we obtain:

$$a = 33.0 \pm 5.0 \; mm.GeV$$

$$b = 8.0 \pm 1.5 \; mm.GeV^{\frac{1}{2}}$$

$$c = 0.9 \pm 0.1 \; mm$$

that are compatible values for the stochastic and electronic noise terms, and an additionnal constant term. Such a constant term is in agreement with what one can expect from the longitudinal fluctuations. Taking $1X_0$ as an order of magnitude of these fluctuations we can estimate the effect of the incident angle on position resolution as

$$dx = X_0 \cdot \sin(3^0)$$

that is 0.9 mm which is actually what we measured.

The Fig. 31 presents the result of the position resolution obtained with the passive preshower in front of the shashlik nonet, and compared with the result without preshower. The result obtained with the preshower in front gives

$$a = 45.6 \pm 3.4 \; mm.GeV$$

$$b = 8.2 \pm 0.4 \; mm.GeV^{\frac{1}{2}}$$

compatible with the result obtained without the preshower, which means that the $3X_0$ preshower has a small effect on the transversal profile measured by the calorimeter.

4.4.2 Position resolution for projective towers

Similar results for the projective tower prototype are shown in Fig. 32 when fitted with the function

$$\sigma_{x,y} = \frac{b}{\sqrt{E}} \oplus c$$

The results are:

$$b = 9.5 \pm 0.3 \ mm.GeV^{\frac{1}{2}}$$

$$c = 0.3 \pm 0.1 \ mm$$

for 0 degree angle and

$$b = 9.9 \pm 0.4 \ mm.GeV^{\frac{1}{2}}$$

$$c = 1.0 \pm 0.1 \ mm$$

at three degrees angle. The same interpretation holds as for the nonet concerning these result, except that a slightly non 0 constant term is already present at 0 degree.

The position resolution for 40 GeV electrons is presented in Fig. 33 as a function of the distance from the tower center. This resolution is going better toward the tower edge since asymmetry is used. The position resolution at the tower edge is about 0.5 mm (beam chamber resolution not unfolded) that is a factor of 3.4 better than at the tower center. No significant difference is found with the preshower in front.

4.4.3 Position resolution of the preshower

The position resolution of the preshower detector has been investigated using several methods. Only three strips were used for position reconstruction to avoid tail fluctuation effect. According to logarithmic method, the position in the preshower plane was calculated as

$$X = X_{max} + K \times ln(\frac{E_{max+1}}{E_{max-1}})$$

where X_{max} denotes the strip coordinate of maximum deposited charge and $E_{max+1}(E_{max-1})$ the charge deposition in neighboring strips. The results are presented in Fig. 34. We obtain:

$$\sigma_x = \frac{2.1}{\sqrt{E}} \oplus 0.4 \ mm$$

for the first plane and

$$\sigma_y = \frac{2.0}{\sqrt{E}} \oplus 0.2 \ mm$$

for the second plane. In these results, the beam chamber resolution has been unfolded. The stochastic terms are almost equivalent for the two planes, while constant terms differ by a factor two. This constant term is mainly due to the shower development fluctuations in the absorbers.

4.4.4 Angular resolution at tower center

The angular resolution of the combined shashlik projective and preshower prototypes is obtained by combining the respective position resolutions. The lever arm between the two measurements was taken as

$$d = (6 + lnE - 3) \times X_0 + 3cm$$

where E is in GeV, X_0 in cm and where 3cm accounts for a reasonable estimate of the gap between the preshower rear face and the shashlik front face. The resulting angular resolution is presented in Fig. 35. One found an angular resolution of 11.3 mrad at 40 GeV. The best description of the data is given by

$$\sigma_\theta = \frac{a}{E} \oplus \frac{b}{\sqrt{E}}$$

with

$$a = 348.5 \pm 29.8 \; mrad.GeV$$

$$b = 48.7 \pm 3.4 \; mrad.GeV^{\frac{1}{2}}$$

at tower center. Also shown are the lines corresponding to

$$\sigma_\theta = \frac{60}{\sqrt{E}} \; mrad$$

and

$$\sigma_\theta = \frac{80}{\sqrt{E}} \; mrad$$

which provide a reasonable frame of the data points.

The performances of the first generation shashlik and preshower prototypes are summarized in Table 2.

4.5 Muon response

Muons data with 225 GeV μ^- have been taken both to calibrate the preshower and to study the shashlik prototypes response to mip. The beam size is very wide and limited by the chambers size to 10×10 cm^2. The signal distribution for muons is presented in Fig. 36 where one observes two Landau distributions. The first peak corresponds to the signal of mip in the scintillator (although at such high energy muons are not really mip). The second peak has a mean energy deposited of 4.9 GeV. It corresponds to the signal of muons hitting the photodiode, as shown in Fig. 37 where the response of these events in the shashlik nonet is plotted as a function of the beam coordinates. One can clearly identify the position and shape of the silicon photodiode. However, the number of events in this peak is only few %, corresponding to the ratio of the scintillator and diode area, and therefore the total energy deposited by mip should be well below 10 GeV, even at the highest background condition at LHC.

	Non projective	Projective
Energy resolution at 0^O without preshower with preshower	 $8.9\%/\sqrt{E} \oplus 0.8\%$ $10.0\%/\sqrt{E} \oplus 0.8\%$	$9.6\%/\sqrt{E} \oplus 0.9\%$
Uniformity of the response After correction		$\pm 3\%$ $\pm 1\%$
Shashlik position resolution at 0^O and at tower center (mm)	$9.3/\sqrt{E} \oplus 37.3/E$	$9.5/\sqrt{E} \oplus 0.3$
Preshower position resolution plane 1 (mm) plane 2 (mm)	$2.1/\sqrt{E} \oplus 0.4$ $2.0/\sqrt{E} \oplus 0.2$	
Estimated angular resolution (mrad)		$48.7/\sqrt{E} \oplus 348.5/E$

Table 2: Shashlik and preshower prototypes performances

5 Monte Carlo simulations

5.1 Geometry used

Simulations were performed using GEANT 3.15 package. The setup was represented by 12 trapezoidal towers with front and rear surface being squares with 52 and 67 millimeters respective sides. Towers were positioned so as to provide about 200 μm air gaps between them; in addition, they were surrounded by layer of light material (carbon was used to reproduce possible glue and wrapping). Towers consisted of 72 pairs of lead-scintillator tiles of 2 and 4 mm respective thickness, providing $26X_0$ depth. Fibres were positioned in lead tiles to take into account their effect on shower development.

Simulations were made also for a shashlik setup with preshower. The preshower consisted of two copper absorbers of 2 and 1 X_0 thickness and two silicon planes of 400 μm thickness. The distance between absorbers was 4 cm and the first silicon plane was placed at the middle. The distance from second absorber to the second silicon plane was 1 cm, and from silicon to shashlik also 1 cm.

Electron beams of 10, 20, 40, 80 and 150 GeV were used. The results presented here were obtained without magnetic field.

5.2 Optical program and usage of maps

To account for light collection effects, the INR/LIP standalone optical simulation program was used. It provided five maps of light collection efficiency for five different tiles whose parameters are listed in Table 3.

Values shown in brackets are presumably the worst possible; they were used in the evaluations of lateral response (section 5.4). The plate sizes were choosen so as to match five equidistant planes in tower depth, the first and the fifth being equal to the first

parameter	value
Size of larger side (square)	52 to 67 mm
Thickness	4 mm
Light absorption length in scintillator	100 cm (20 cm)
Scintillator refraction index	1.59
Hole diameter	1.4 mm
Number of fibres	36
Fibre diameter	1.2 mm
Fibre refraction index	1.5
Light absorption length in fibre	100 cm
Light re-emission length in fibre	0.15 mm
Efficiency of light reflection:	
from plate large side cover (diffuse)	0.8 (0.7)
from plate small side cover (specular)	0.8 (0.4)
total inner reflection	0.93

Table 3: Optical parameters

and the last in the tower. At each step of GEANT shower development, the position dependent light collection efficiency was calculated using interpolation between suitable maps. Cerenkov radiation in the fibres was simulated by increasing corresponding values in the maps. Light attenuation was then taken into account for both possible light paths (direct or via fibre loop) to photosensor. Electronic noise was not considered.

5.3 Energy resolution

5.3.1 shashlik only

Energy resolution was estimated using simulations with the beam targeted at the 10 by 10 mm square at the center of front surface of module number 7. The air gap between the modules was 200 μm and modules coating consisted of carbon of 250 μm thickness, resulting in a total distance from lead to lead of 700 μm. The resolution at 150 GeV was 0.96%. All points are shown in Fig. 38 together with the unconstrained two-parameters fit that includes stochastic and constant terms. The result obtained is

$$\frac{\sigma_E}{E} = \frac{9.2\%}{\sqrt{E/GeV}} \oplus 0.7\%$$

Constraining stochastic term at 9.5% (result obtained from experimental data) we got constant term of 0.6%.

5.3.2 Combined shashlik and preshower

To evaluate the combined shashlik and preshower energy resolution, we fitted the weighted sum of silicon plane 1, plane 2 and shashlik responses to find the corresponding coefficients. The fits were made separately for each beam energy using different methods :

- only shashlik information (passive preshower),
- shashlik + energy deposition in 3 most significant strips in each silicon plane,
- shashlik + 5 strips,
- shashlik + total energy depositions in each plane.

Results are shown in Fig. 38. The best results in combined preshower+shashlik resolution were obtained using the total energy deposition in each plane.

5.4 Lateral response

The shape of the lateral response is given in Fig. 39 for the 40 GeV beam. In the same figure we show also the curve obtained using the presumably worst parameters of light collection in the tiles (as given in brackets in section 5.2). After a simple correction using the fitted global over-module shape was applied, the lateral response shows a non-uniformity within $\pm 1\%$, except for the region of projective (central) gap. The response in this region is shown in Fig. 40 (average value and sigma). The energy resolution is shown for different beam positions and energies in Fig. 41. Though statistics is rather poor, no strong effect is seen at the non-projective gap region (the effective gap position corresponds to center of shower being in the gap; it moves from 5.6 cm at 10 GeV to 5.8 cm at 150 GeV). This region is shown in more detail in Fig. 42. It represents the sigma of the energy deposition in scintillator tiles for 40 GeV electron beam targeted at the points near non-projective gap with 1 mm step. Two sets of points were obtained with different module coating thicknesses (100+100 and 250+250 μm of carbon plus 200 μm of air in both cases); correction for lateral leakage was applied to energy deposition values. For the thicker coating, about 1 % decrease of the average value is seen at the gap position; local sigma increases are also seen in both cases. From this result one can estimate that in the gap region ($\approx$ 1cm width) the constant term is increased by 0.5%.

5.5 Energy leakage

For a 4 by 3 towers prototype setup, most part of the energy leakage was found to be due to the limited lateral size of detector (table 4). For 40 GeV, only 17% of the leakage is longitudinal. Overall leakage rates obtained by the simulations for incident electron energies of 10 and 150 GeV are shown in Fig. 43 as a function of beam distance from the central gap.

Table 4: Energy leakage. Beam targeted on 20 by 20 mm square at the center of tower 7.

Beam energy, GeV	Energy leak, %			
	Total		Lateral	Longitudinal
	average	σ		
10	2.47	0.35	2.20	0.27
20	2.51	0.29	2.16	0.35
40	2.55	0.24	2.07	0.42
80	2.64	0.20	2.08	0.56
150	2.80	0.19	2.01	0.79

5.6 Effect of non-projectivity of scintillator tiles

In the simulations, the scintillator tiles were represented by layers filling completely the shape of tower (i.e., having truncated pyramidal shape). However, information of energy deposition and light collection was obtained also on rectangular parts of scintillator layers to allow for the estimation of the effect of non-projective tiles. In fig. 44 the average fraction of energy deposited in the projective parts of layers is shown. It amounts to 0.6% at non-projective gap position. The distributions of this value are presented in fig. 45 separately for beam targeted on central part of module 7 and on the non-projective gap. We estimate that in the gap region ($\approx$ 1cm width) parallelepipedical scintillator tiles make an additional contribution to the constant term of 0.25%.

6 Conclusions

The results presented in this note confirm and enlarge the previous one obtained for the nonet of non projective towers with silicon photodiode readout. The energy resolution is

$$\frac{\sigma_E}{E} = \frac{(460 \pm 6)MeV}{E} \oplus \frac{(8.9 \pm 0.5)\%}{\sqrt{E}} \oplus (0.8 \pm 0.1)\%$$

The shower position resolution is

$$\sigma_{x,y} = \frac{37.3 \pm 2.6}{E} \oplus \frac{9.3 \pm 0.4}{\sqrt{E}}(mm)$$

at tower center.

A new prototype of projective towers with photomultiplier readout has been successfully tested. The results are in agreement with the ones obtain with the nonet. The energy resolution is found to be

$$\frac{\sigma_E}{E} = \frac{(9.6 \pm 0.8)\%}{\sqrt{E}} \oplus (0.9 \pm 0.1)\%$$

in good agreement with Monte Carlo calculations. The uniformity of the response is within $\pm 3\%$. Such non uniformity corresponds to Monte Carlo prediction with bad

optical parameters values. It is shown to be correctable to $\pm 1\%$ using the asymmetry measured by the calorimeter itself ('in situ' calibration).

A first generation silicon strips preshower has been tested in conjunction with the shashlik prototypes. When combined with the calorimeter position measurement, we obtain an angular resolution at tower center of the order of

$$\sigma_\theta = \frac{70}{\sqrt{E}}(mrad)$$

Appendix 1: exhaustive list of recorded data in summer 93

- may 93 runs
  - *nonet calibration*, 40 GeV, narrow beam, about 3000 events per run
  - *nonet energy scan*, 15,20,40,80,120,150 GeV, narrow beam, about 5000 events per run
  - *nonet horizontal scan 1*, X=713.5-780.5, Y=917.5, 40 GeV, wide beam, about 10000 events per run
  - *nonet horizontal scan 2*, X=713.5-780.5, Y=925.8, 40 GeV, wide beam, about 10000 events per run,
  - *nonet horizontal scan 1* with $3X_0$ *Cu* in front, X=713.5-780.5, Y=917.5, 40 GeV, wide beam, about 10000 events per run
  - *nonet horizontal scan 2* with $3X_0$ *Cu* in front, X=713.5-780.5, Y=925.8, 40 GeV, wide beam, about 10000 events per run
  - *nonet energy scan* with $3X_0$ *Cu* in front, 15,20,40,80,120,150 GeV, narrow beam, about 10000 events per run
  - *projective* prototype *calibration*, 40 GeV, narrow beam, about 10000 events per run
  - *projective* prototype *horizontal scan 1*, X=731.5-813.5, Y=873, 40 GeV, wide beam, about 5000 events per run
  - *projective* prototype *energy scan*, 10,15,20,40,80,120,150 GeV, narrow beam, about 10000 events per run
  - *projective* prototype *vertical scan*, X=780.5, Y=831-915, 40 GeV, wide beam, about 5000 events per run
  - *projective* prototype *horizontal scan 2*, X=731.5-820.5, Y=878, 40 GeV, wide beam, about 5000 events per run
  - *projective* prototype with *preshower energy scan*, 10,15,20,40,80,120,150 GeV, narrow beam, about 10000 events per run
  - *projective* prototype with *preshower uniformity scan in T7*, 40 GeV, wide beam, about 5000 events per run
  - *projective* prototype with *preshower uniformity scan in T6*, 40 GeV, wide beam, about 5000 events per run
- august 93 runs
  - *nonet calibration*, 40 GeV, narrow beam, about 5000 events per run
  - *nonet energy scan* at $\theta_z = 0$ *degree*, 15,20,40,80,120,150 GeV, narrow beam, about 5000 events per run

- *nonet energy scan* at $\theta_z = 3$ *degrees*, 15,20,40,80,120,150 GeV, narrow beam, about 5000 events per run
- *nonet horizontal scan 1* at $\theta_z = 3$ *degrees*, X=751-780.5, Y=913, 40 GeV, wide beam, about 10000 events per run
- *nonet horizontal scan 2* at $\theta_z = 3$ *degrees*, X=755-784, Y=918, 40 GeV, wide beam, about 10000 events per run
- *nonet* with *preshower energy scan* at $\theta_z = 0$ *degree*, 15,20,40,80,120,150 GeV, narrow beam, about 10000 events per run
- *preshower calibration* run, 225 GeV μ, about 10000 events per run
- *projective* prototype *calibration*, 40 GeV, narrow beam, about 5000 events per run
- *projective* prototype *energy scan* at $\theta_z = 0$ *degree*, 10,15,20,40,80,120,150 GeV, narrow beam, about 5000 events per run
- *projective* prototype *energy scan* at $\theta_z = 3$ *degrees*, 10,15,20,40,80,120,150 GeV, narrow beam, about 5000 events per run
- *projective* prototype *energy scan in T6* at $\theta_z = 0$ *degree*, 10,15,20,40,80,120,150 GeV, narrow beam, about 5000 events per run
- *projective* prototype *energy scan in T6* at $\theta_z = 3$ *degree*, 15,20,40,80,120,150 GeV, narrow beam, about 5000 events per run

Acknowledgments

We would like to thank all engineers and technicians from the collaboration laboratories that have been involved in the work described in this note. The data presented were taken with the RD5 DAQ and beam setup and we are grateful to our colleagues from RD5 and in particular G. Bencze, F. Szoncso and C. Wultz who made our running conditions possible and easy. Finally, we are grateful to the SPS staff and in particular N. Dobble for providing assistance in understanding the beam line during our tests.

References

1. C. Seez et al., in Proc. of Aachen workshop 1990, eds. G. Jarlskog and D. Rein, CERN 90-10, vol.III (474). See also C. Seez et al., in CMS-TN 92-56.

2. H. Fessler et al., Nucl. Inst. and Meth. A228 (1985) 303 and Nucl. Inst. and Meth. A240 (1985) 284. B. Loher et al., Nucl. Inst. and Meth. A254 (1987) 26. G.S. Atoyan et al., Nucl. Inst. and Meth. A320 (1992) 144.

3. CERN-DRDC RD36, 'A combined shashlik + preshower detector for LHC', J. Badier et al., CERN-DRDC 93-28 (1993), *CERN, Ecole Polytechnique, JINR Dubna, ITEP Moscow, IHEP Protvino, INR Moscow, LIP Lisbon, Imperial College, RAL and Brunnel collaboration*

4. CMS Letter of Intent, CERN/LHCC 92-3/I1 (1992).

5. CMS Status Report and Milestones, CERN/LHCC 93-48 (1993).

6. J. Badier et al., Shashlik calorimeter beam-test results, CMS-TN 93-66, INR-821/93, X-LPNHE/93-4 (1993).

7. E. Gushin et al., Fast low noise hybrid amplifier for the CMS calorimetry, CMS-TN 93-108 (1993).

8. A. Karar, Readout of WLS fibres in shashlik calorimeter by a matrix of PIN photodiodes and noise evaluation, CMS-TN 93-96 (1993) and Proceedings of the IV Internationnal Conference on Calorimetry in High Energy Physics, La Biodala, Isola d'Elba, Italy, September 19-25, 1993.

9. E. Beuville et al., Nucl. Inst. and Meth. A288 (1990) 157.

10. J. Badier et al., Position and angular resolution with the Shashlik calorimeter, CMS-TN 93-65 (1993).

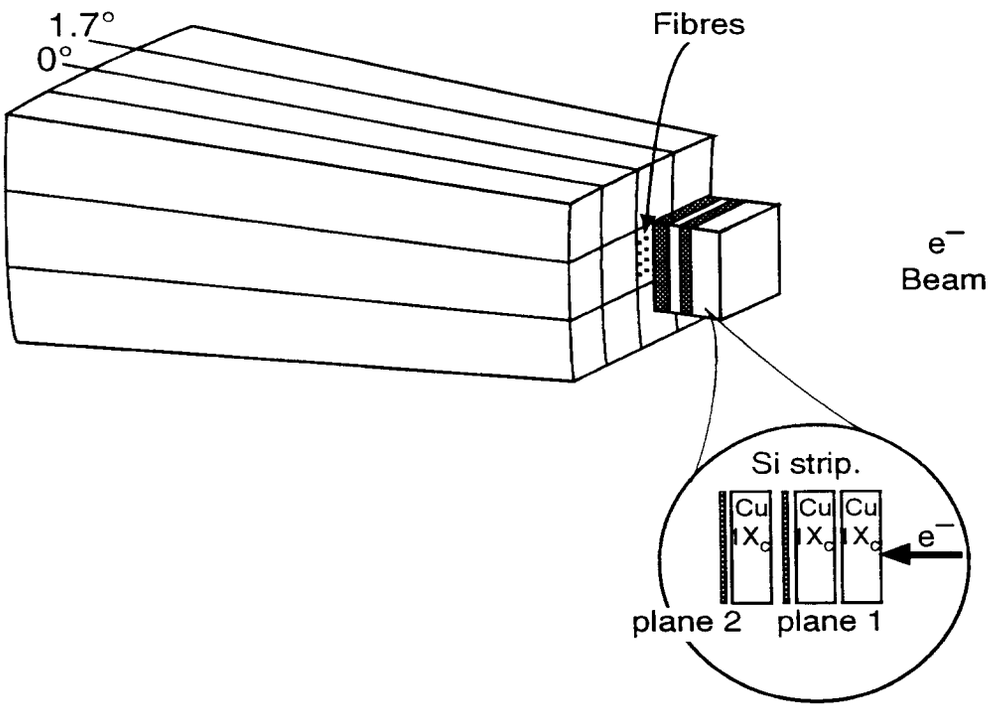

Figure 1: Layout for projective and preshower prototypes

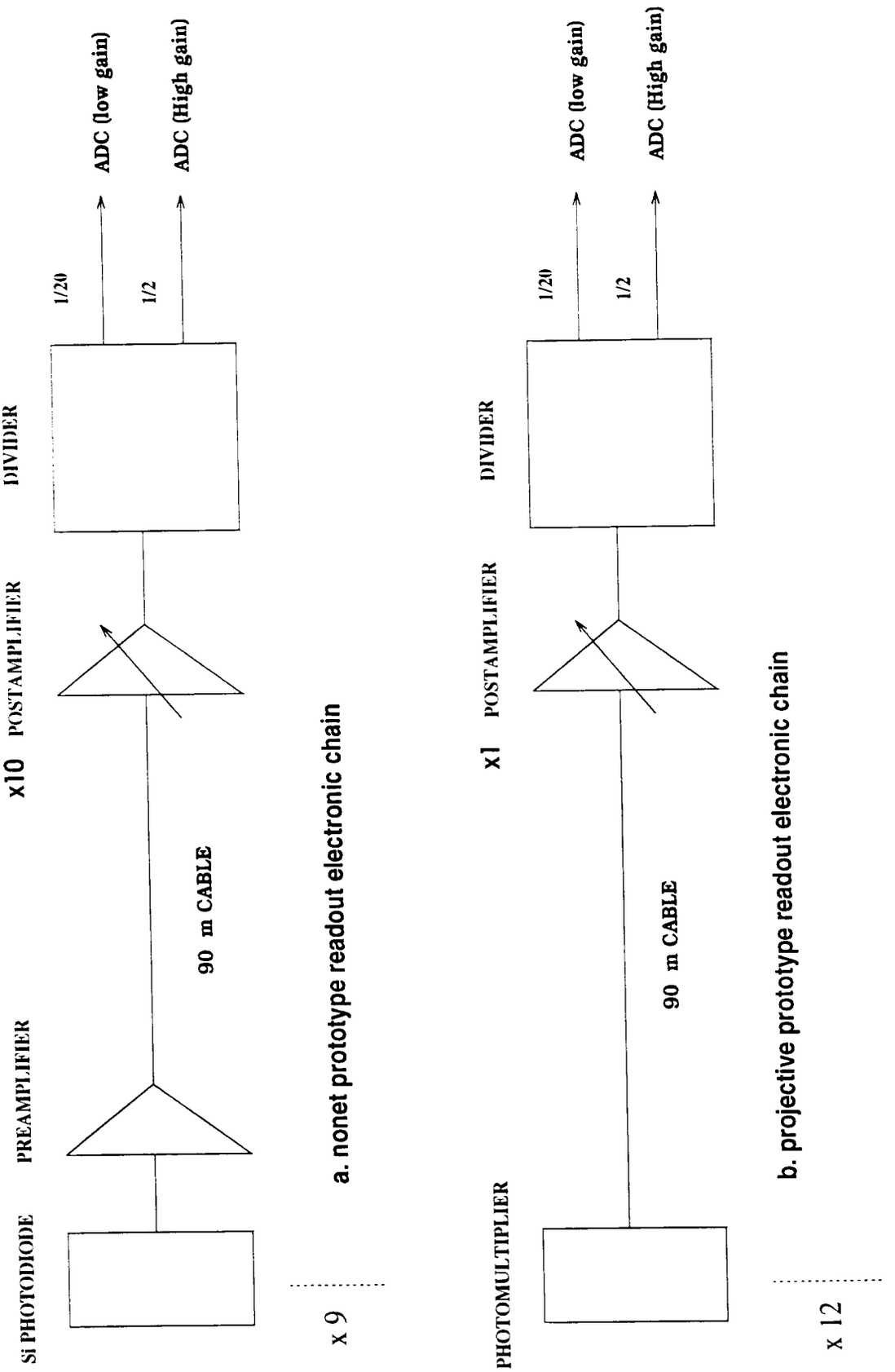

Figure 2: Shashlik readout electronic chain

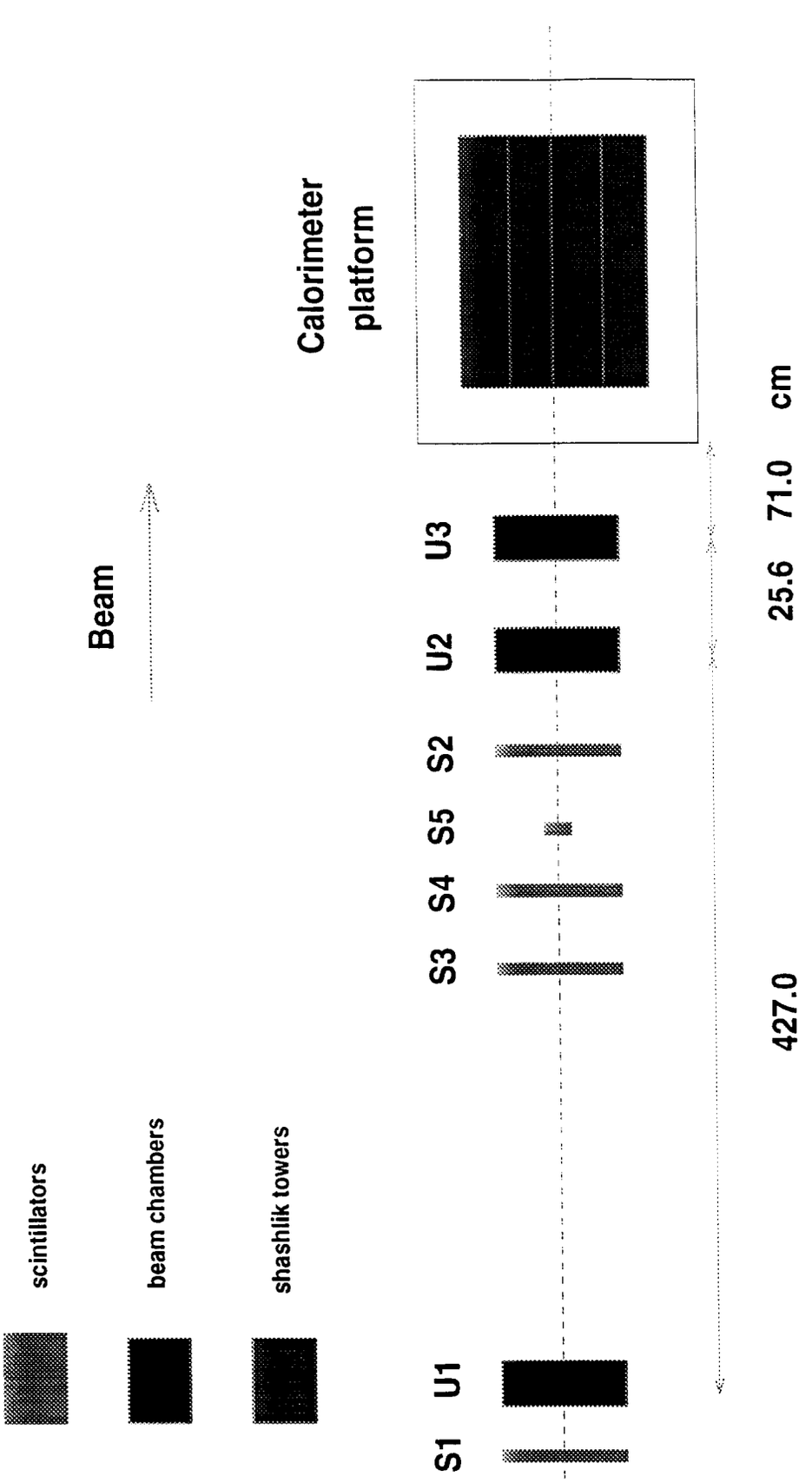

Figure 3: Shashlik beam line setup

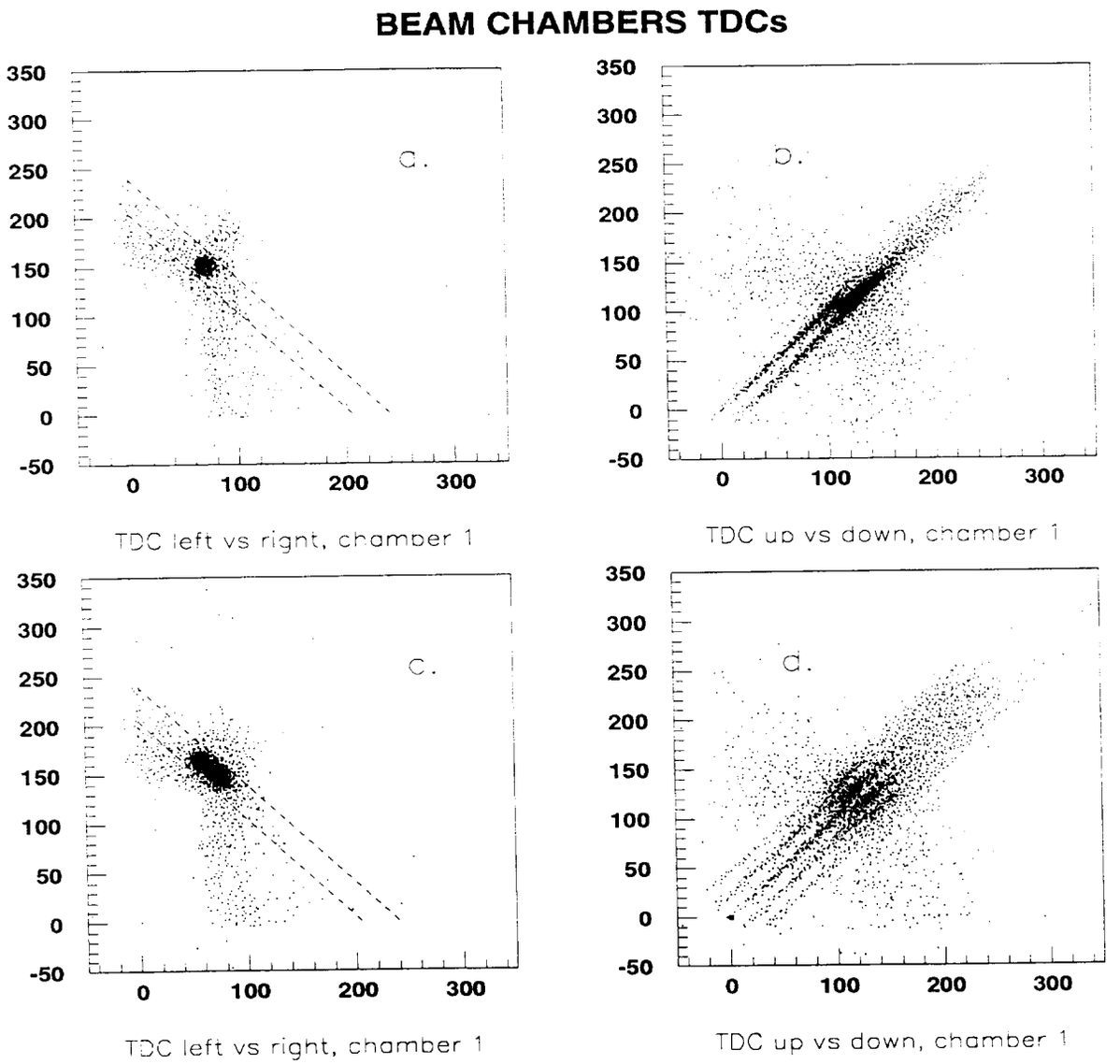

Figure 4: Beam chamber U1 TDCs raw distributions for narrow beam: a. left vs right, b. up vs down; and for wide beam: c. left vs right and d. up vs down. Units are nanoseconds. Dashed lines indicate cuts on TDCs sum (see text).

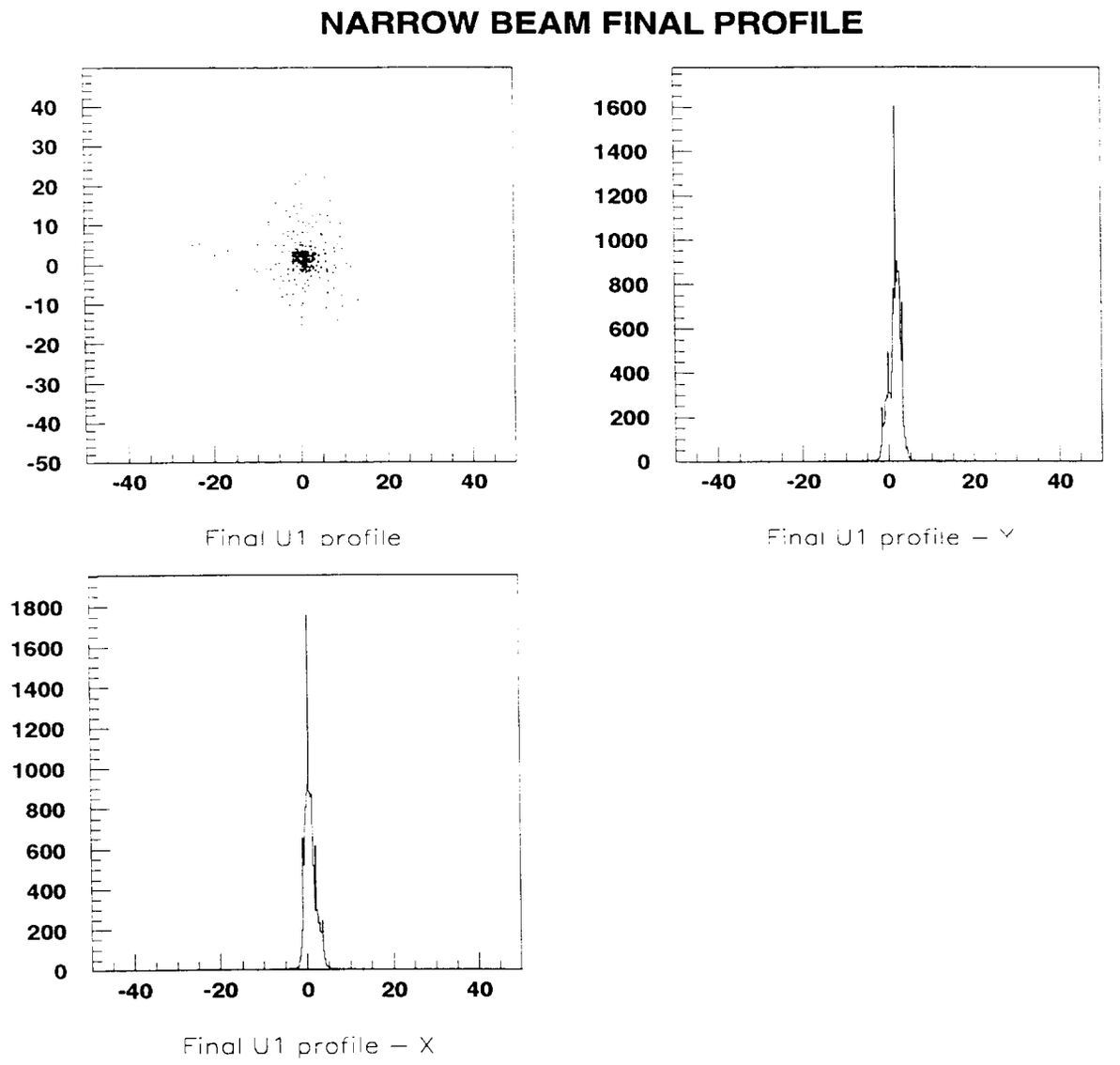

Figure 5: Beam chamber final U1 profile for narrow beam. Units are millimeters.

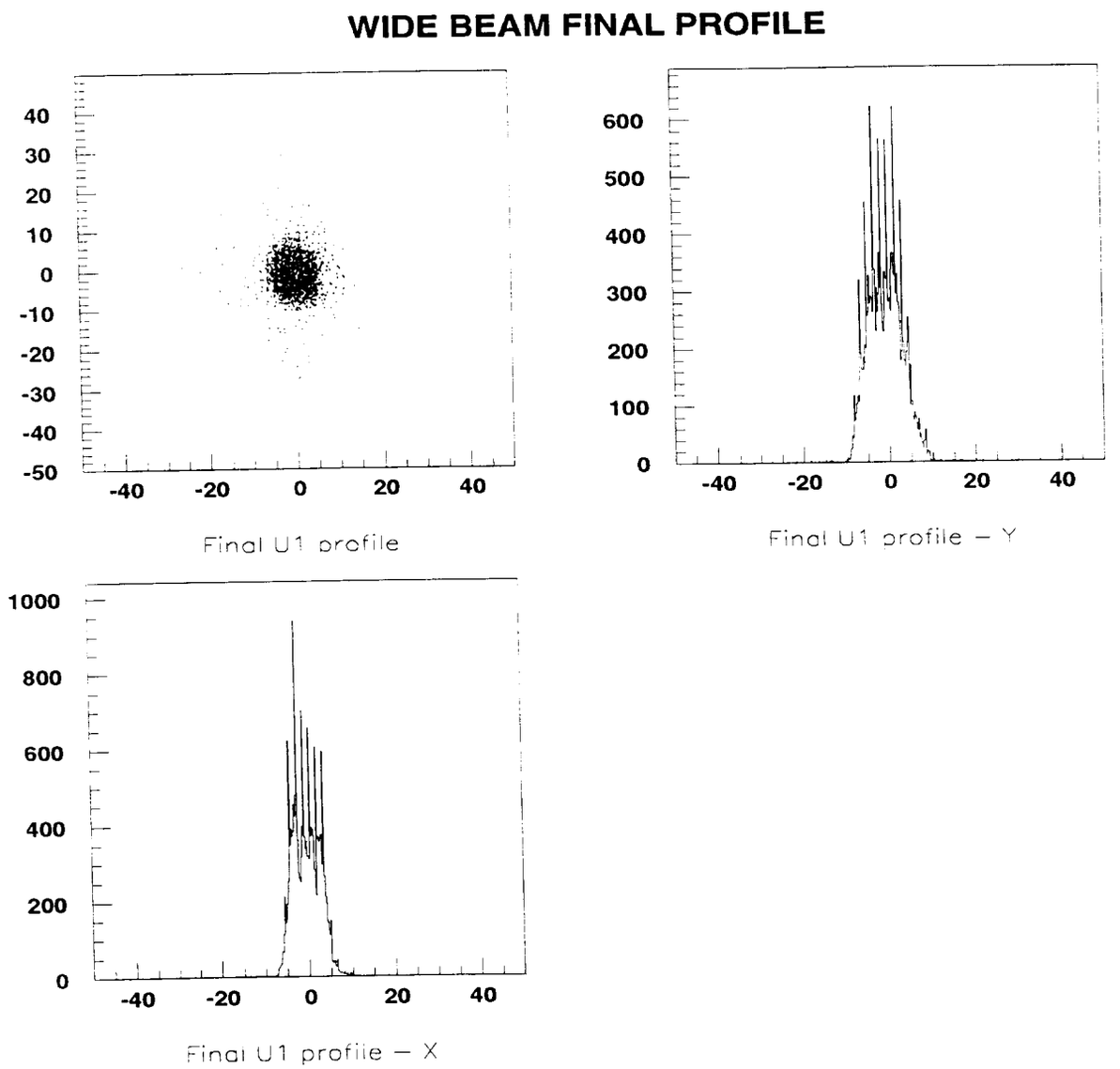

Figure 6: Beam chamber final U1 profile for wide beam

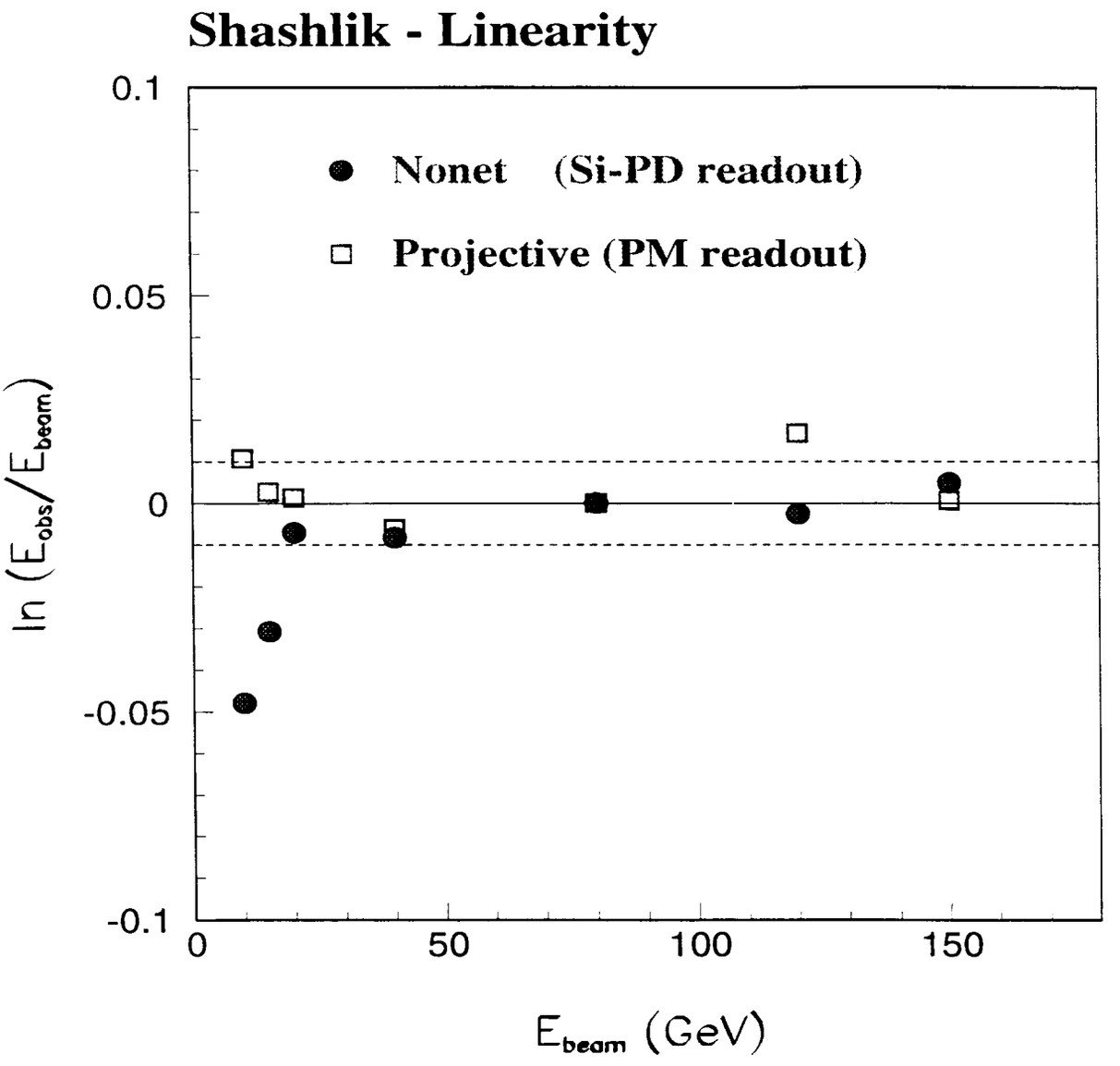

Figure 7: Shashlik nonet and projective prototypes linearity

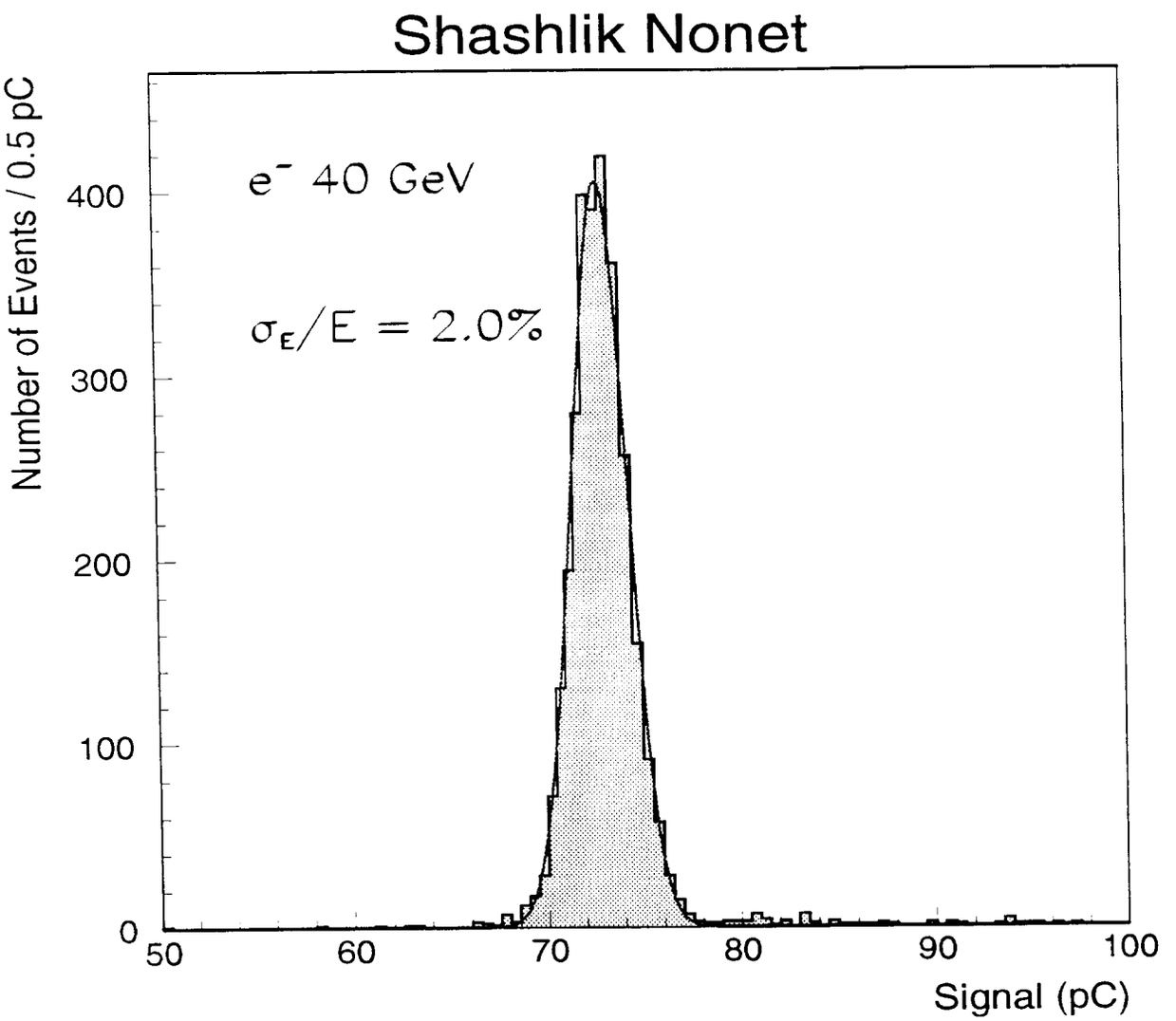

Figure 8: Shashlik nonet energy distribution for 40 GeV e^-

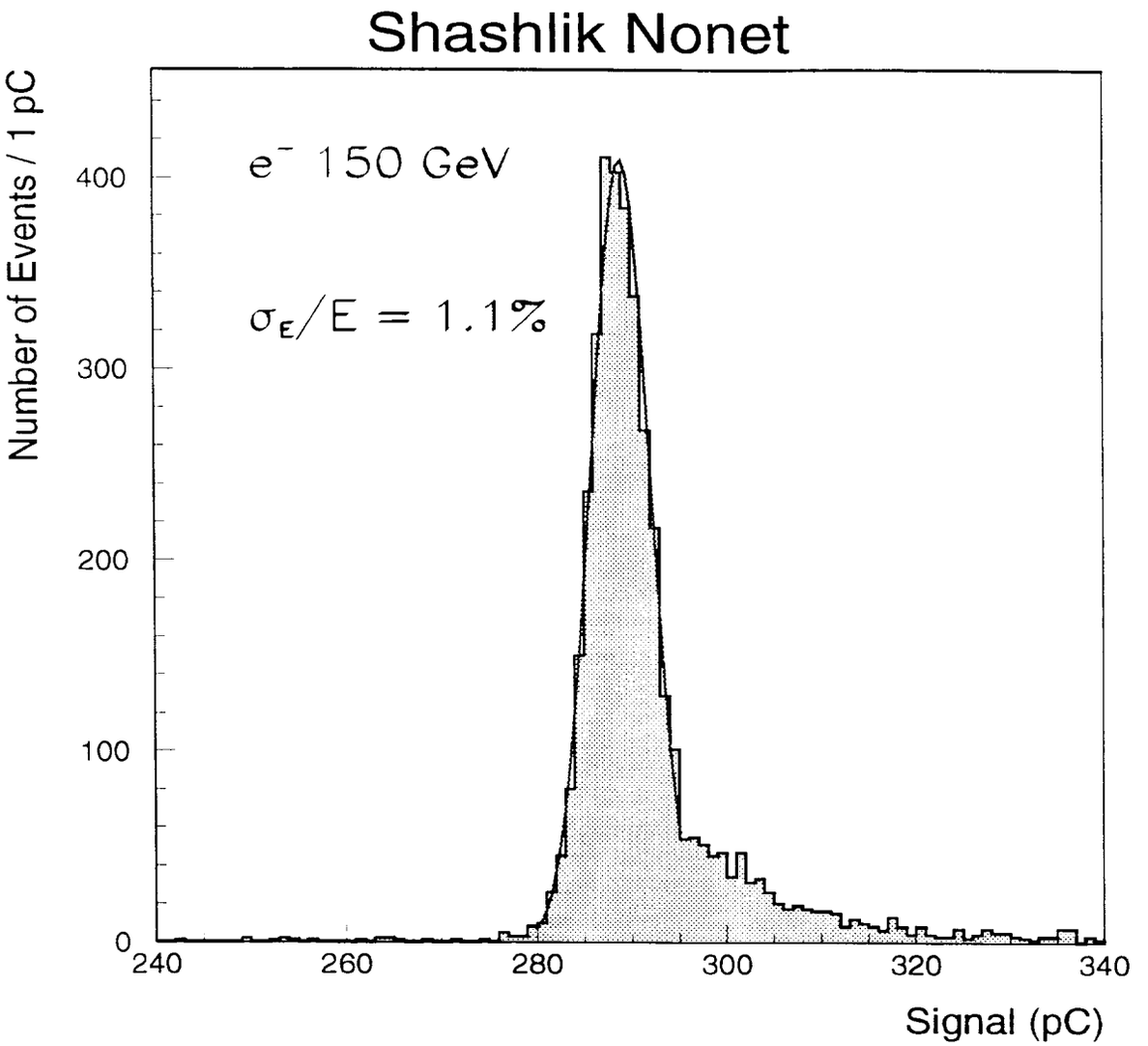

Figure 9: Shashlik nonet energy distribution for 150 GeV e^-

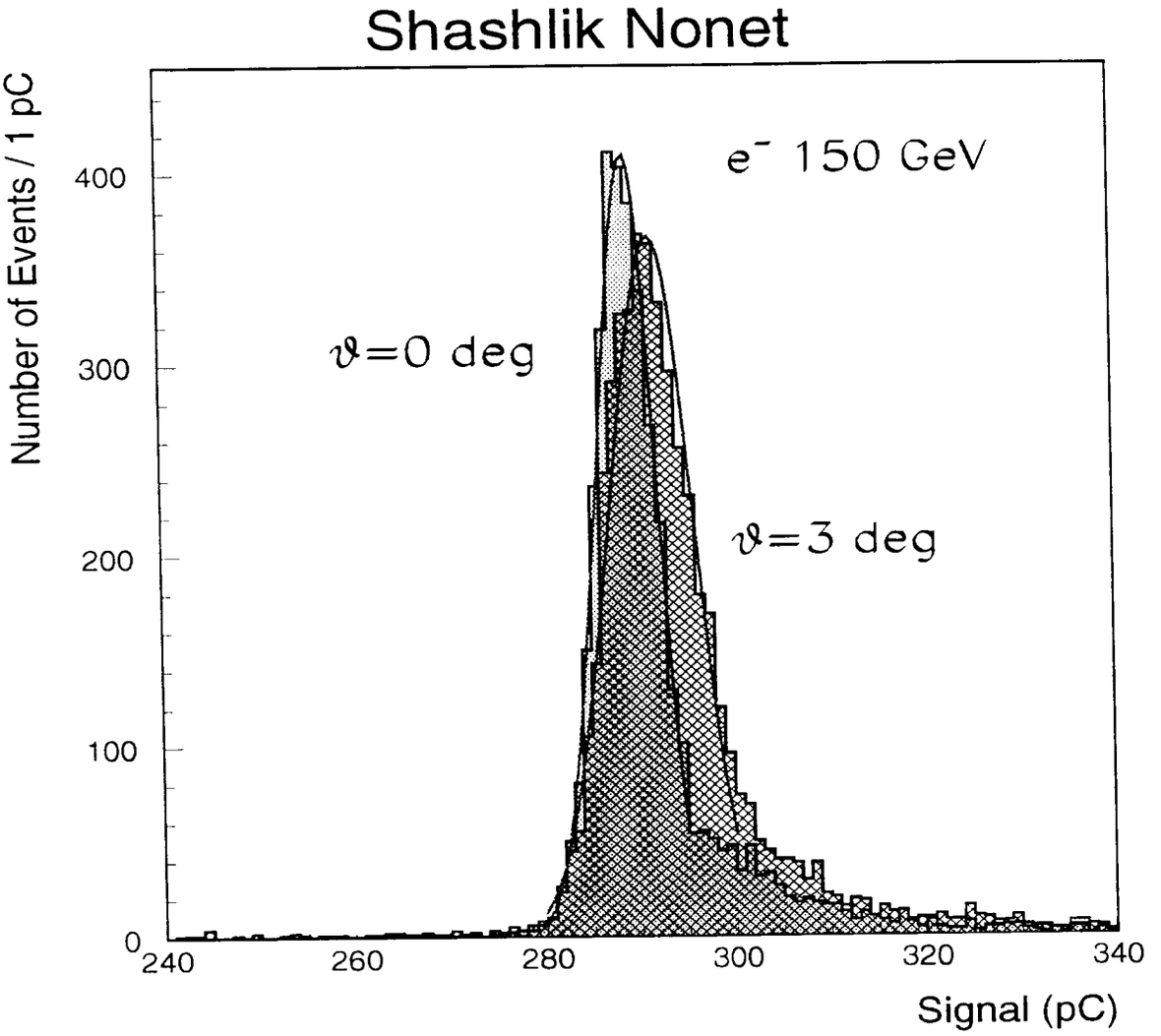

Figure 10: Shashlik nonet energy distribution for 150 GeV e^- at $\theta_z = 3$ degrees, compared with same at $\theta_z = 0$ degree

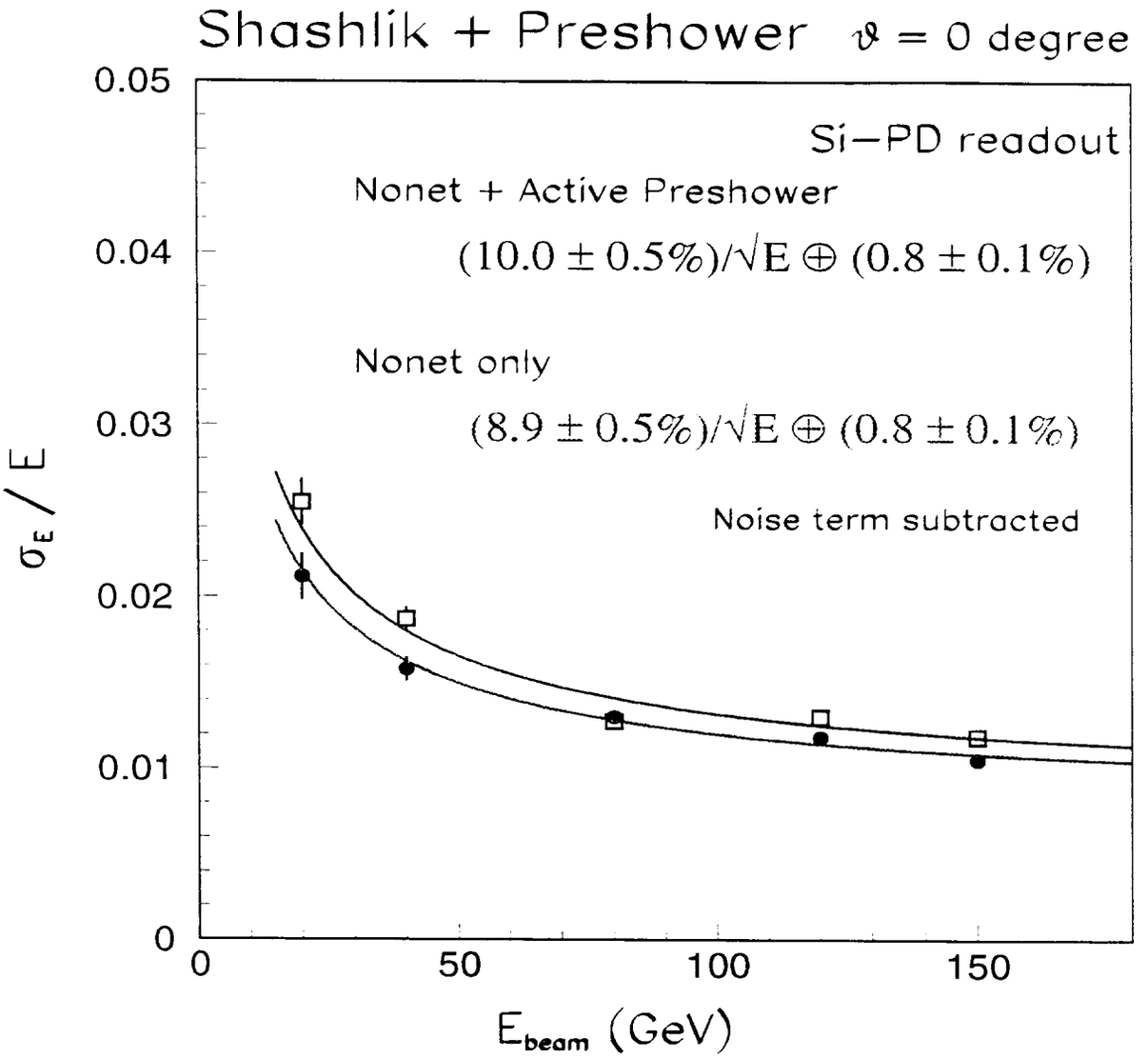

Figure 11: Energy resolution for the nonet as a function of beam energy. Lines are quadratic fits described in text

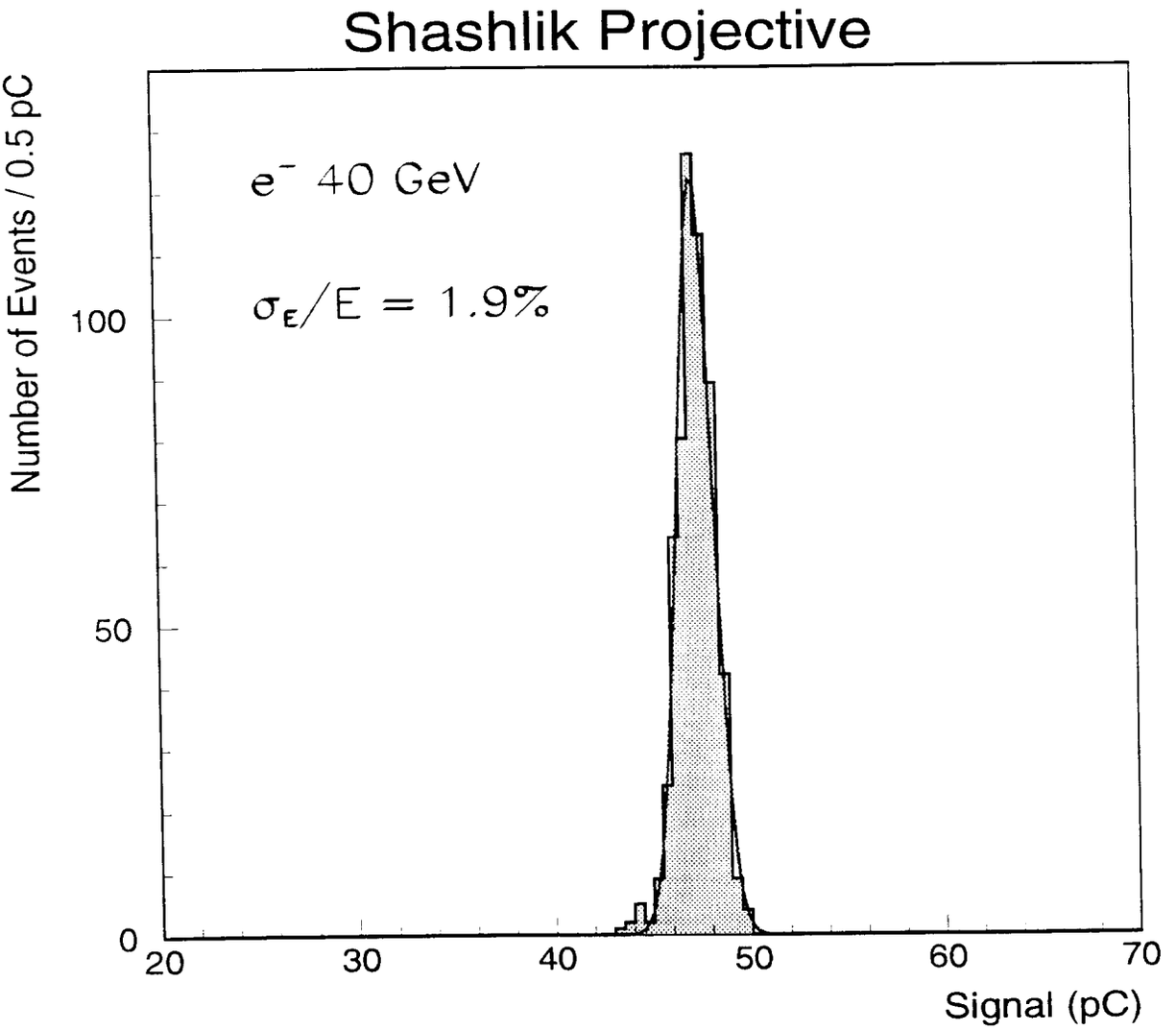

Figure 12: Shashlik projective prototype energy distribution for 40 GeV electrons

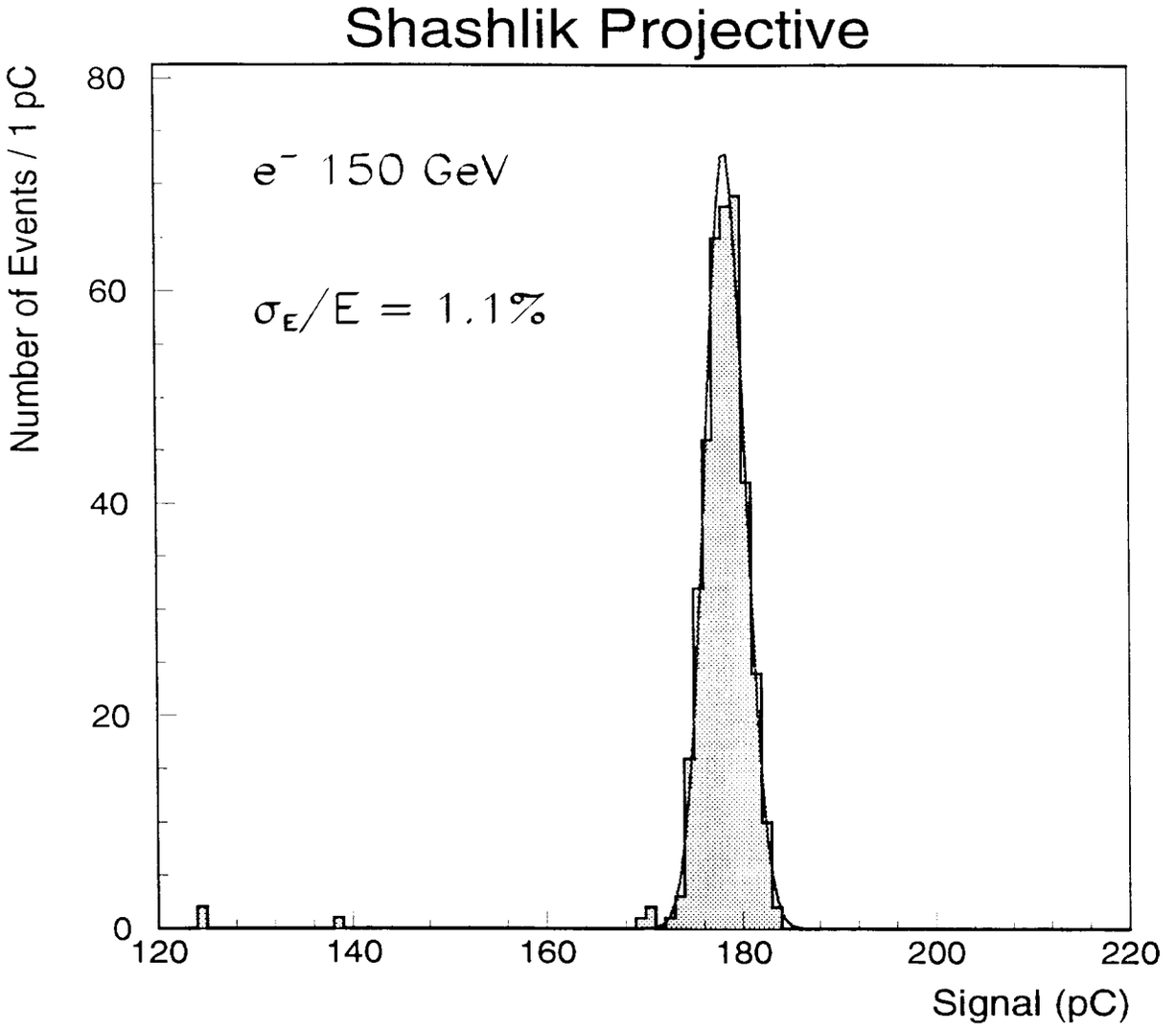

Figure 13: Shashlik projective prototype energy distribution for 150 GeV electrons

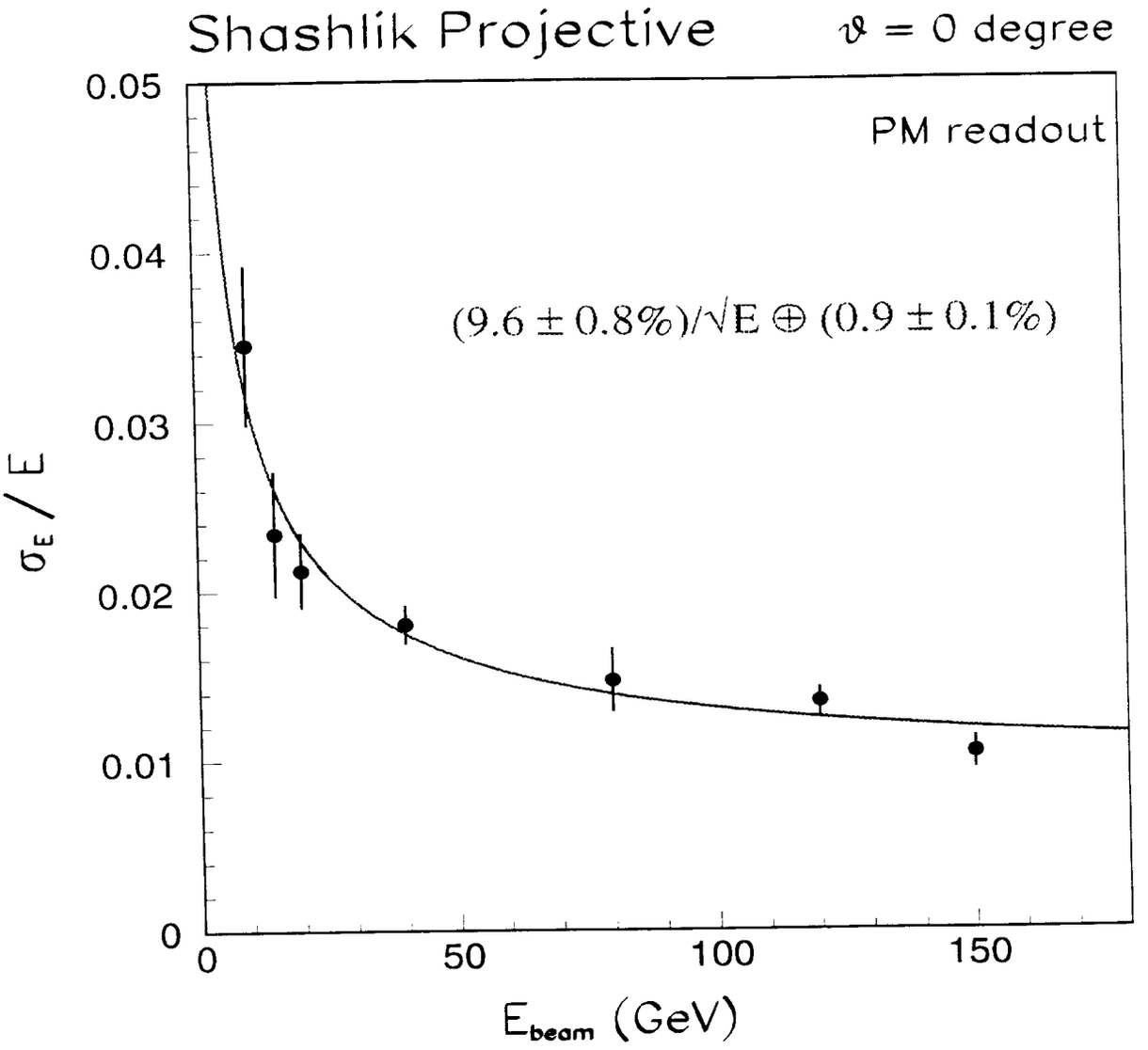

Figure 14: Energy resolution for the projective prototype as a function of beam energy. Line is a quadratic fit as decribed in text.

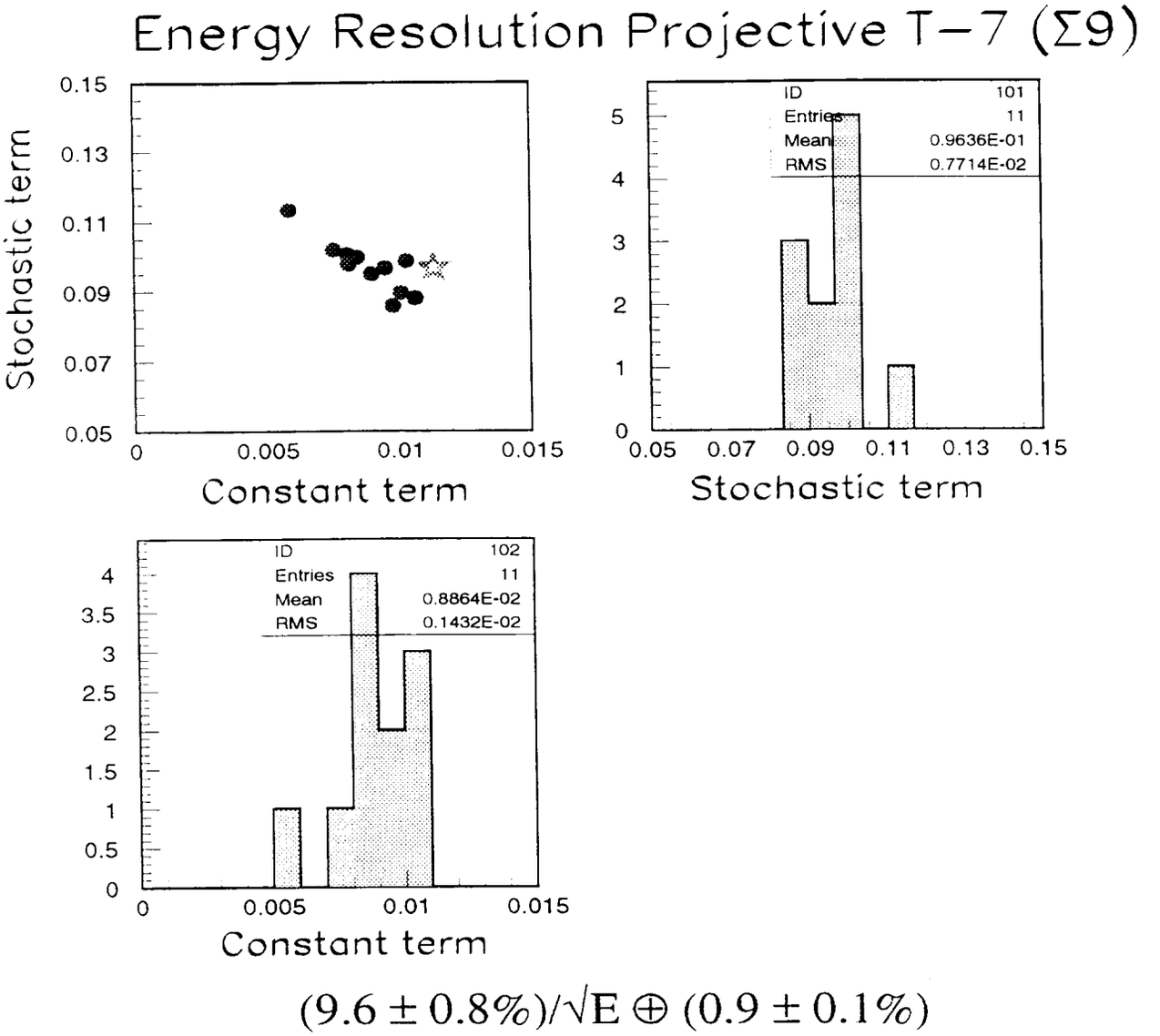

Figure 15: Fitted values of energy resolution parameters for the projective prototype when subdividing the beam size in bins of 1.5×1.5 mm^2. The correlation between the fitted parameters is also shown.

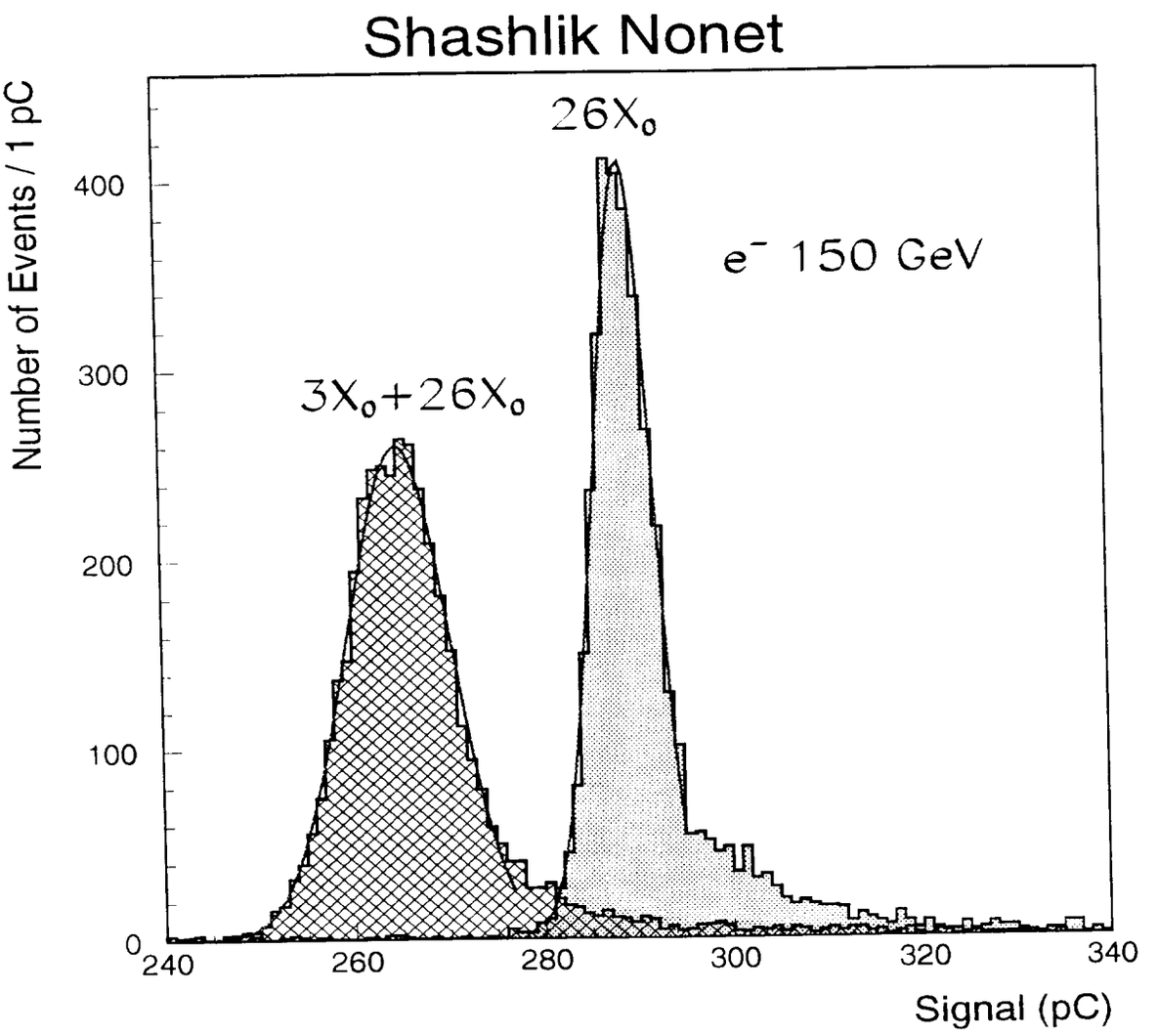

Figure 16: Energy resolution for the nonet with passive preshower in front compared with the result without preshower for 150 GeV e^-

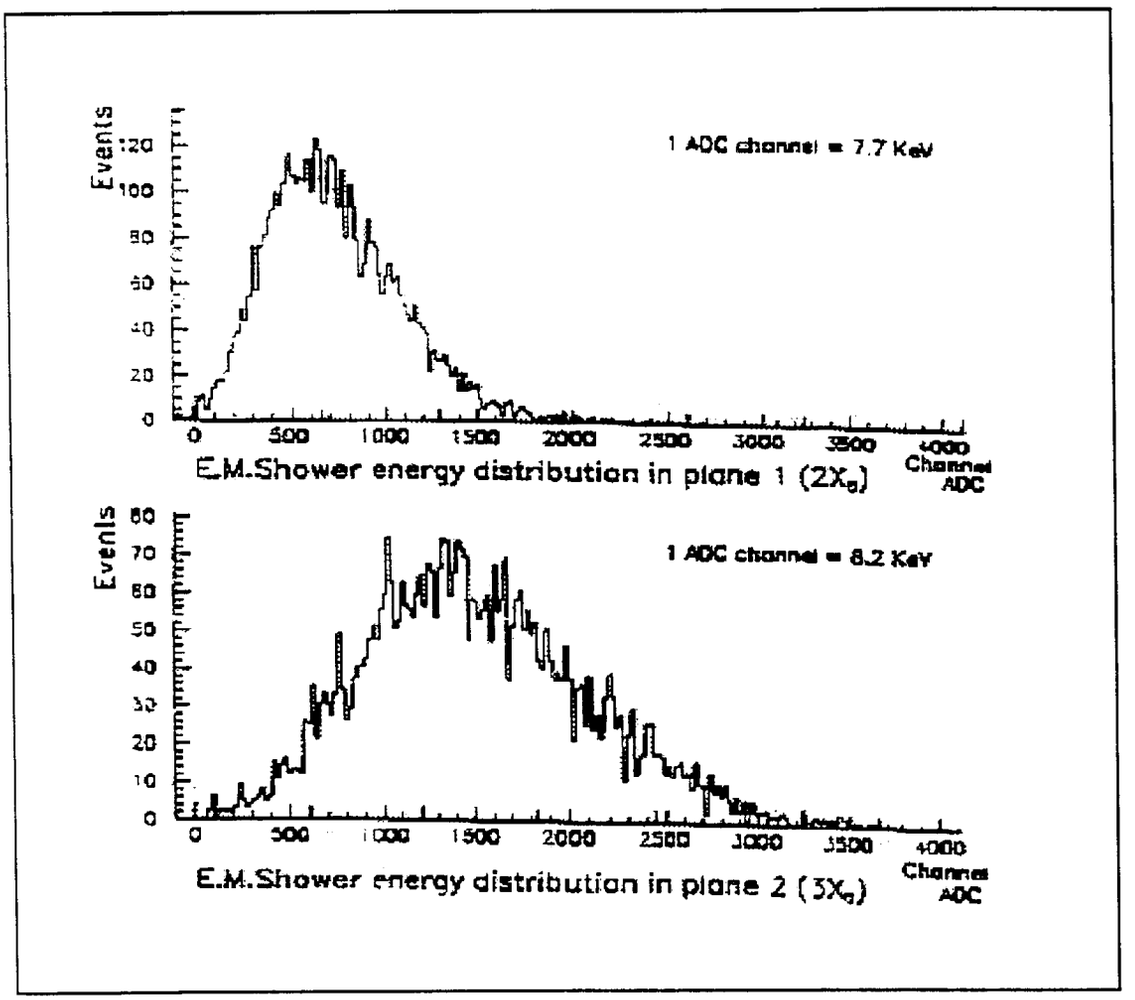

Figure 17: Energy distributions of the two preshower planes for 40 GeV e^-

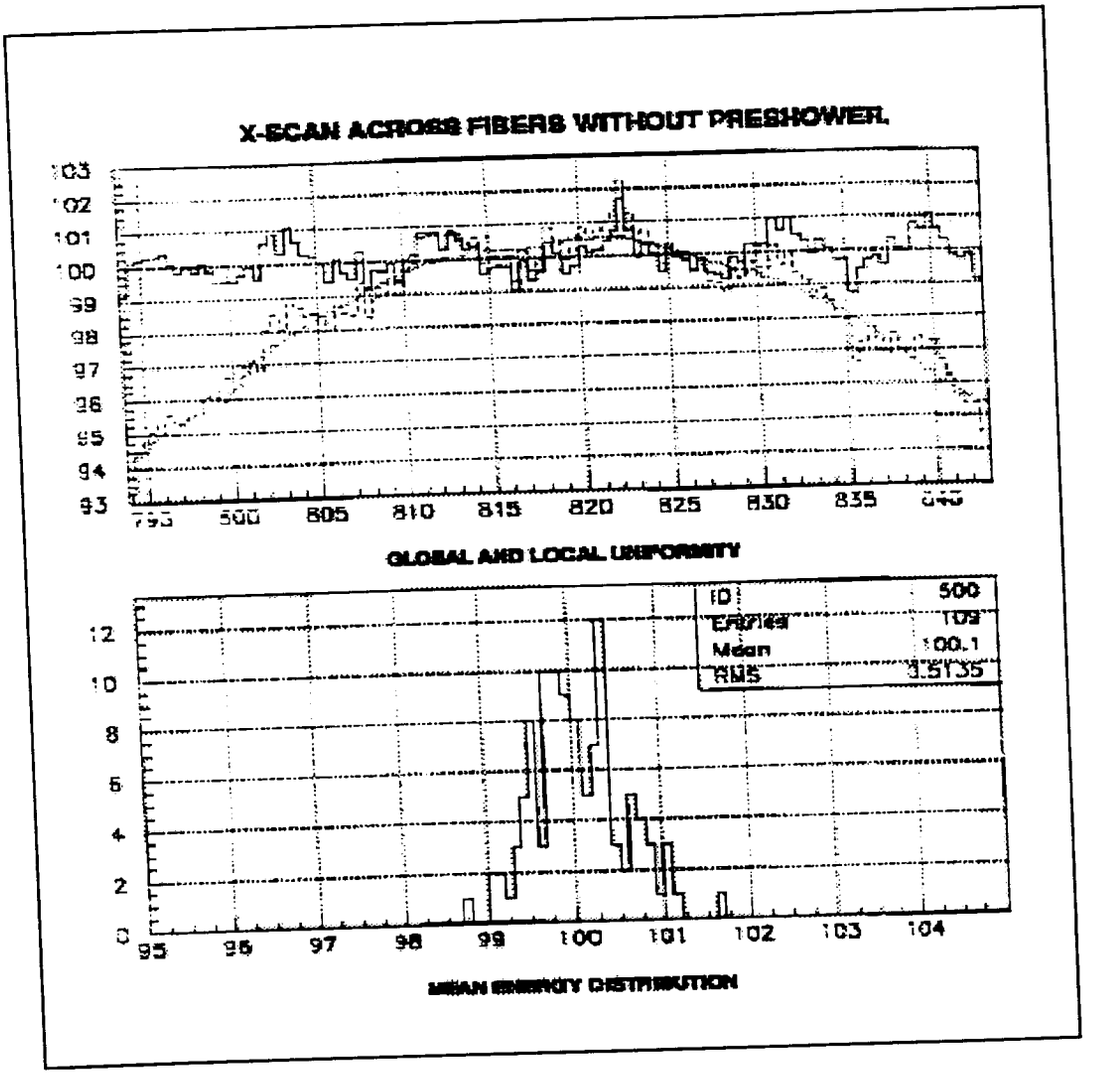

Figure 18: X scan across fibres for projective prototype: mean energy response as a function of horizontal beam position and residual after fitting the dependence (on top); distribution of the mean response after the fit of the position dependence (on bottom)

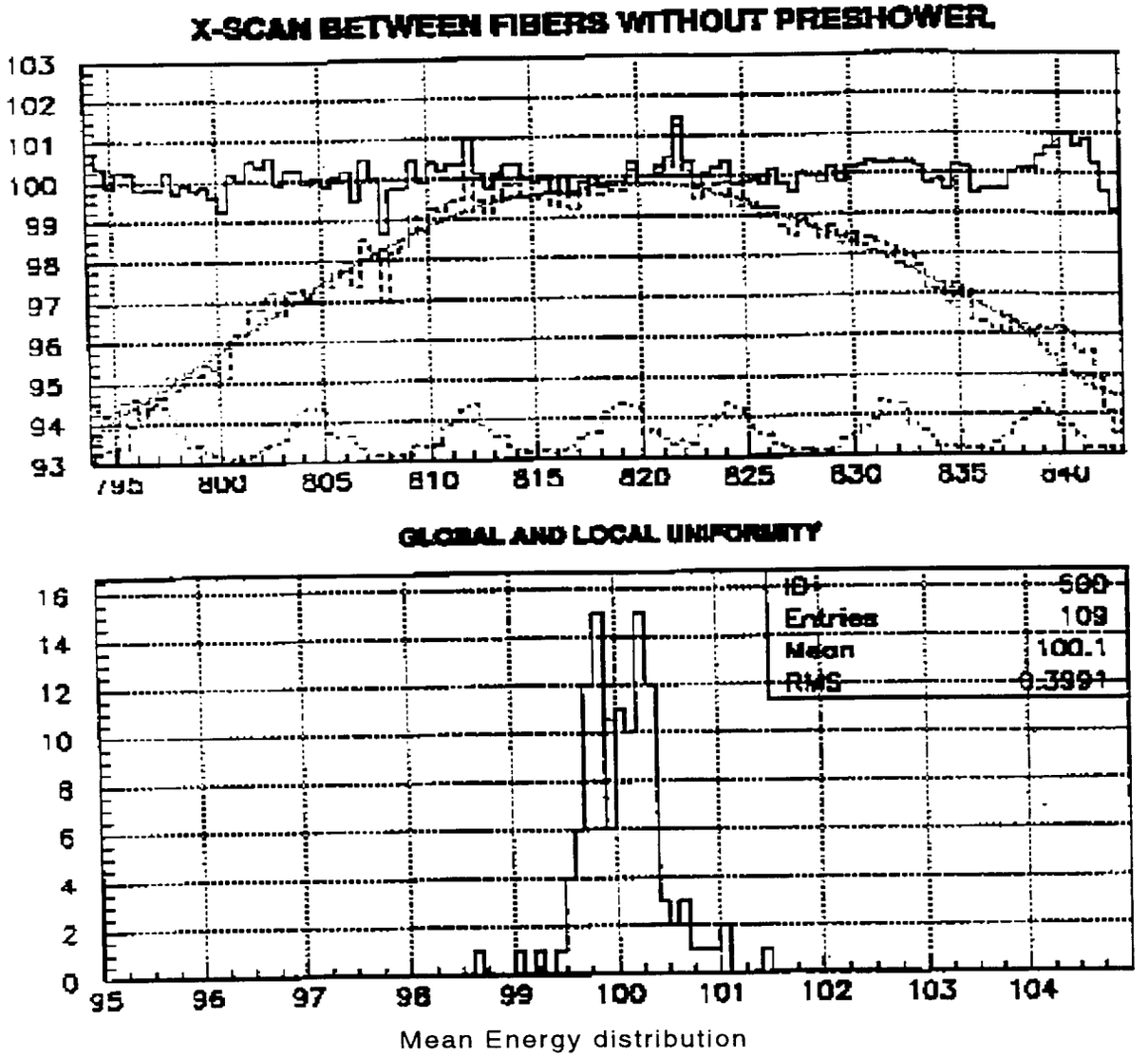

Figure 19: Same as Fig. 18 for X scan between fibres

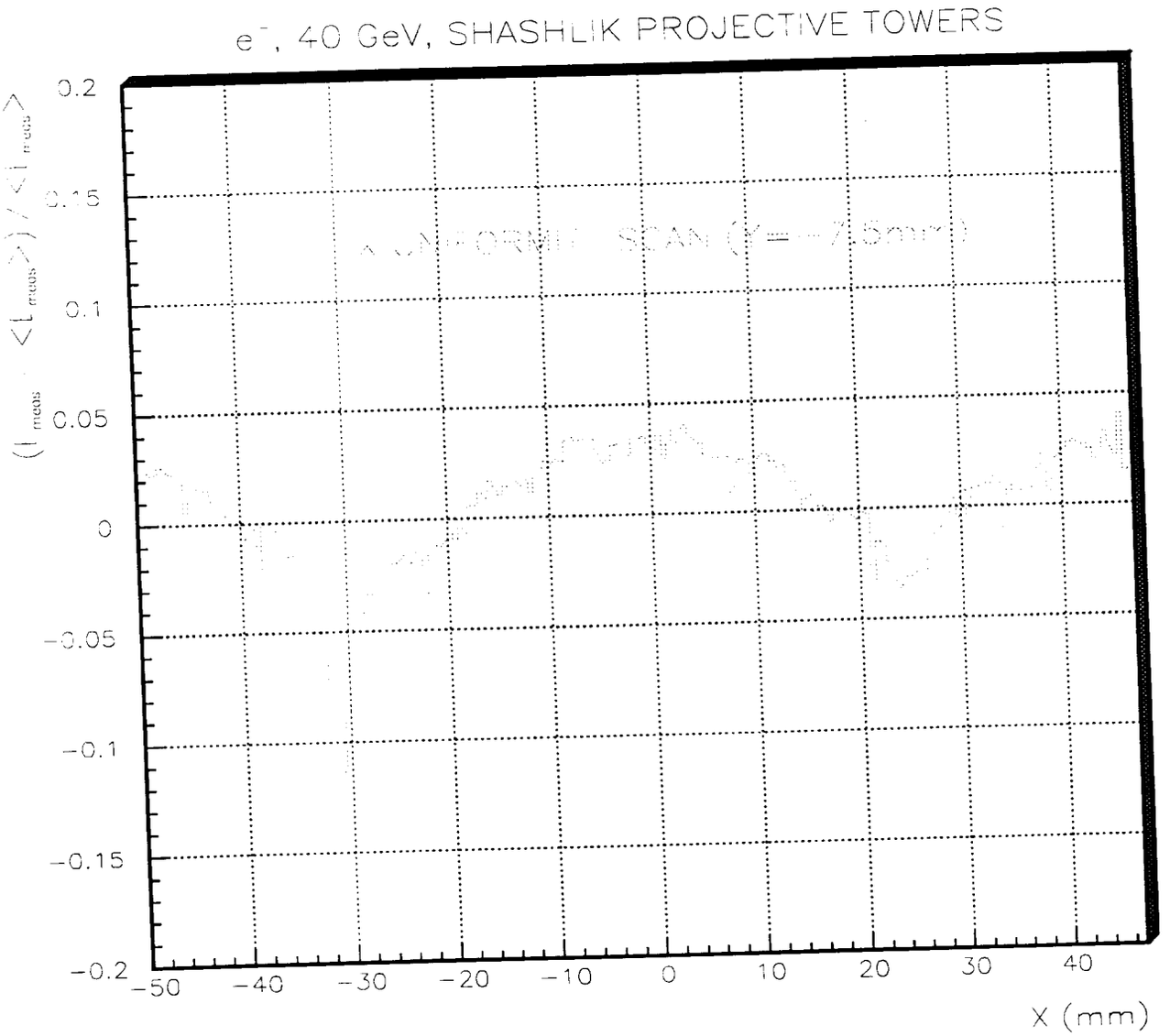

Figure 20: X scan across fibres for projective prototype from T6 center to T8 center

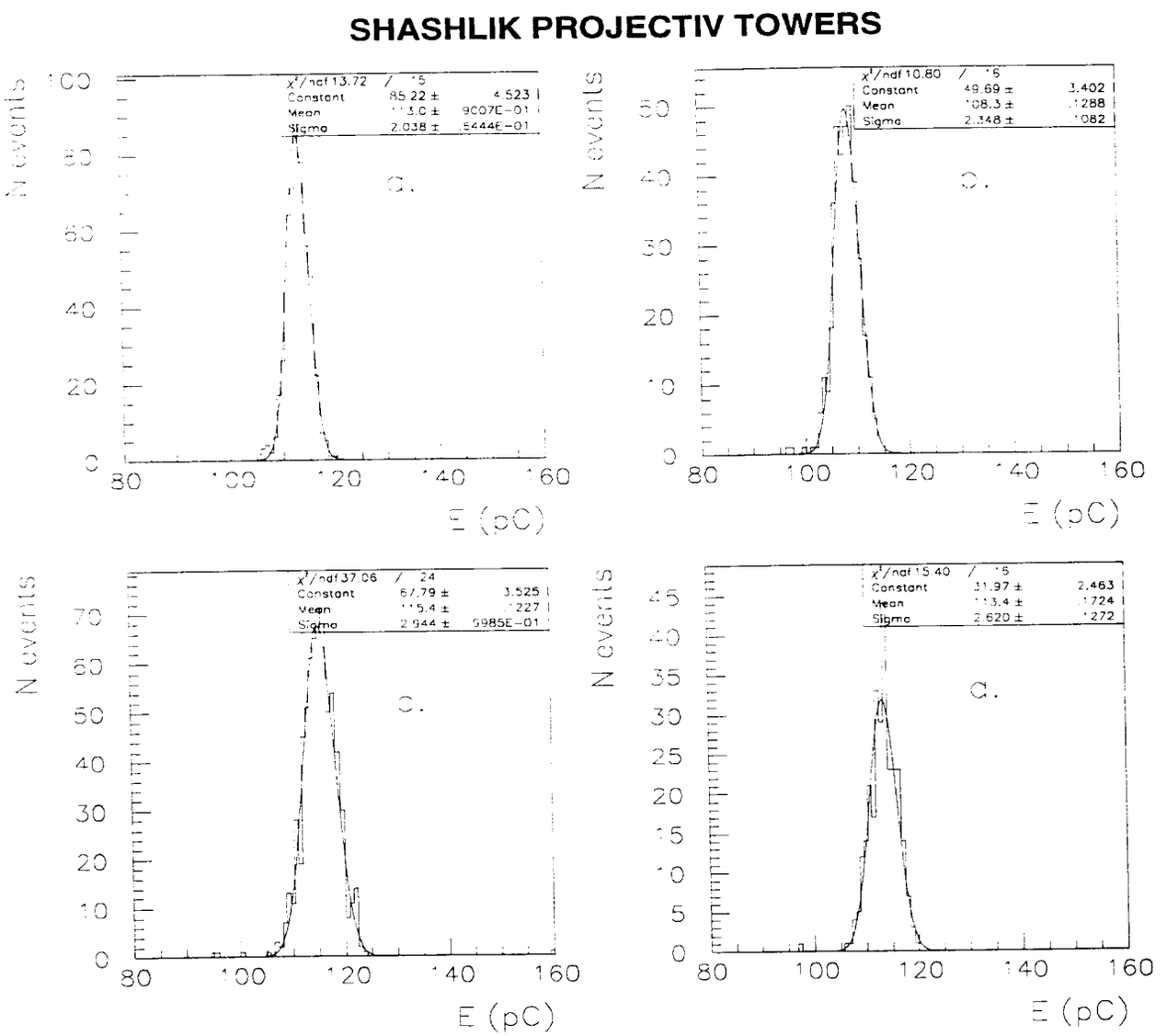

Figure 21: Energy resolution for 40 GeV e^-, without preshower: a. at tower center; b. in tilted crack; and with preshower: c. at tower center; and d. in tilted crack.

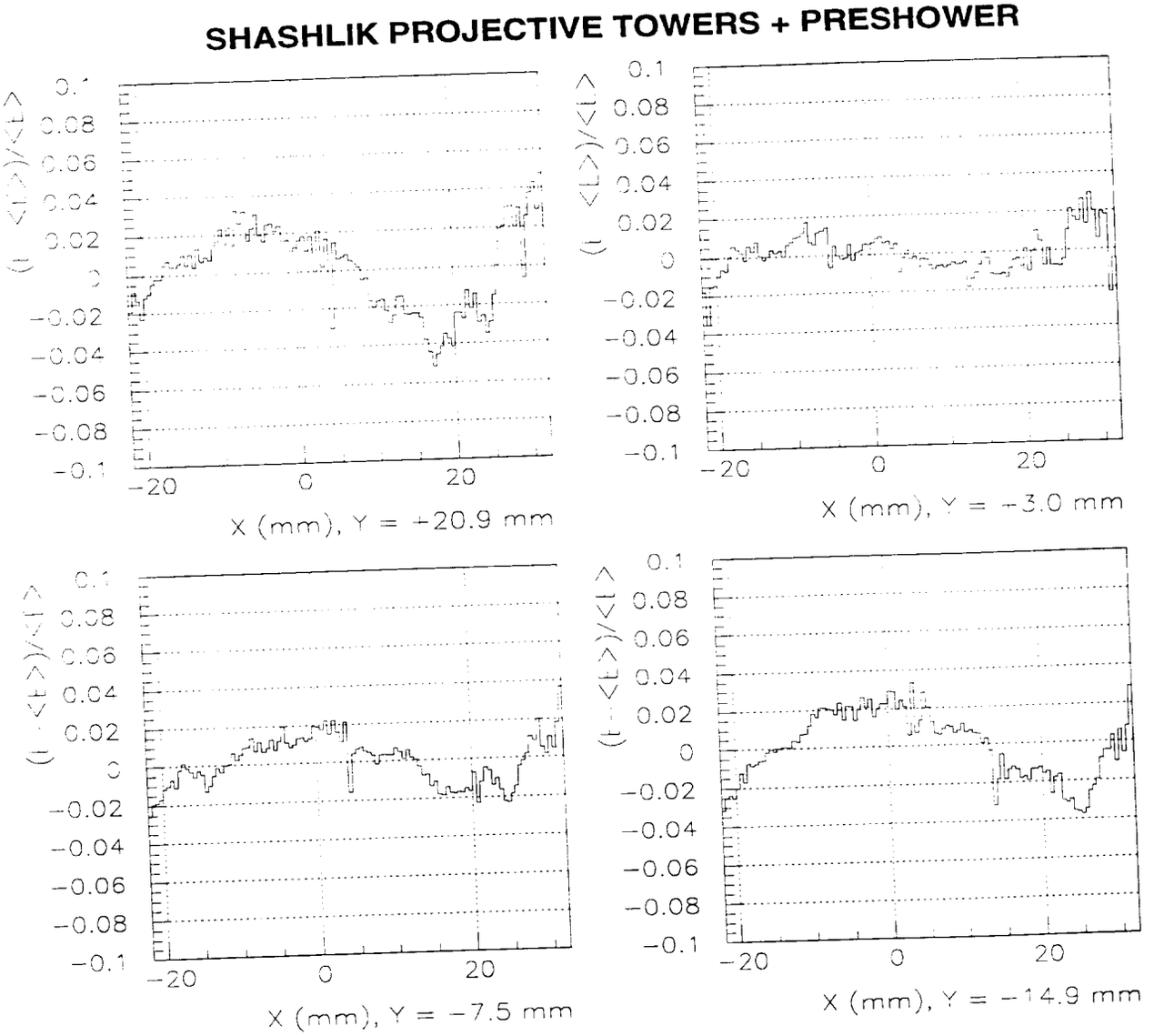

Figure 22: X scans for projective prototype with preshower for various Y positions

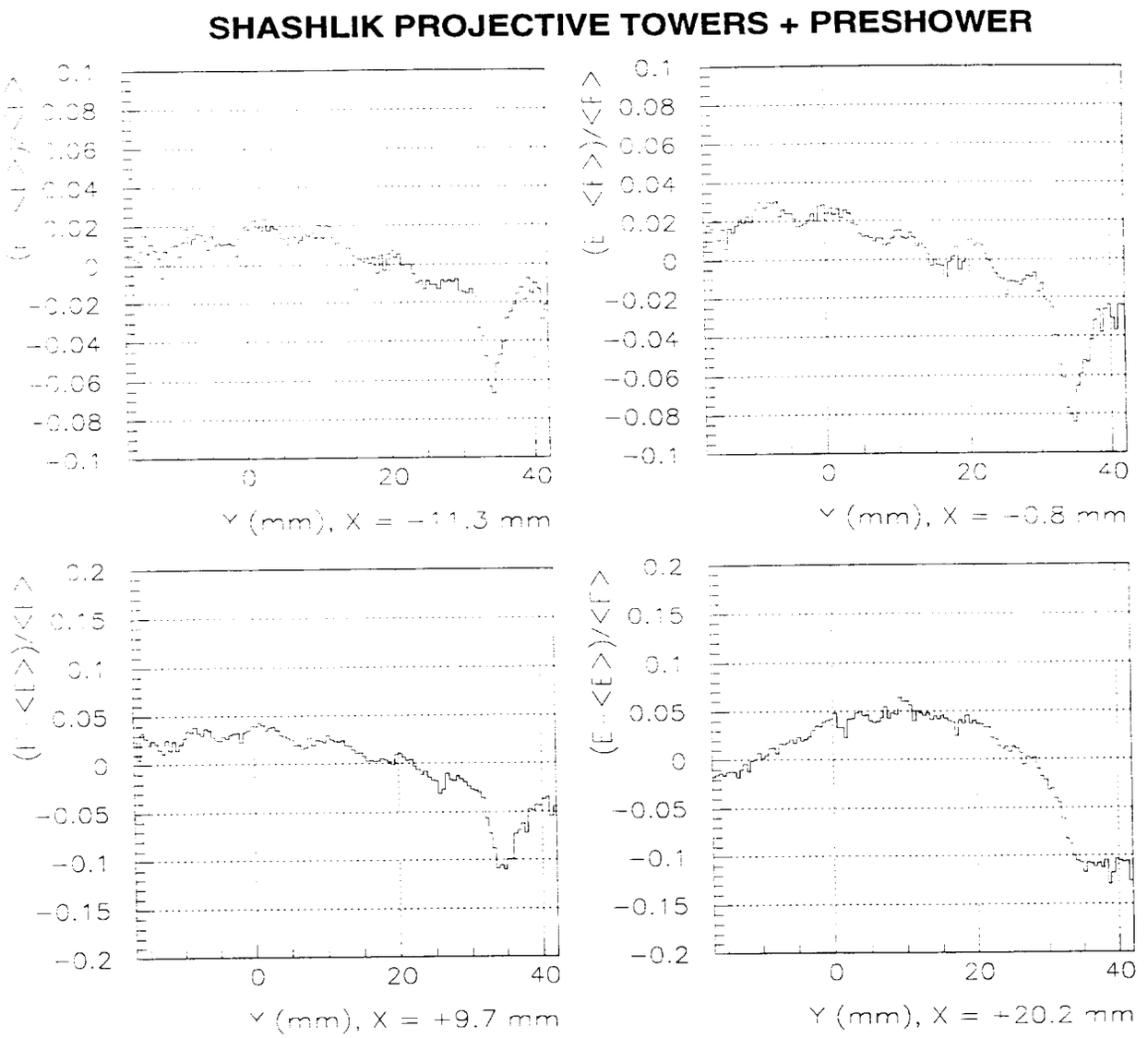

Figure 23: Y scans for projective prototype with preshower for various X positions

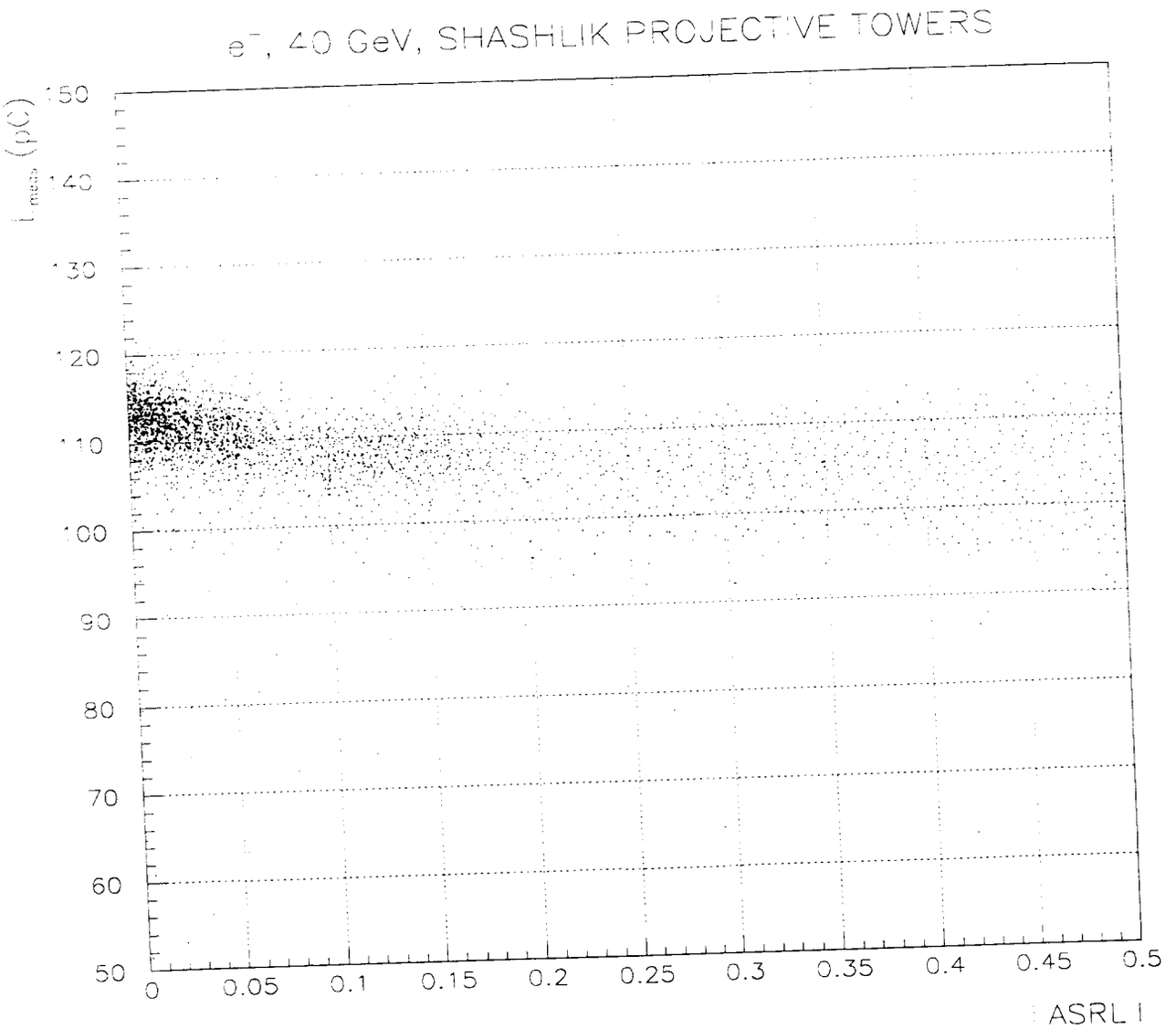

Figure 24: Correlation between asymmetry and measured energy for 40 GeV electrons

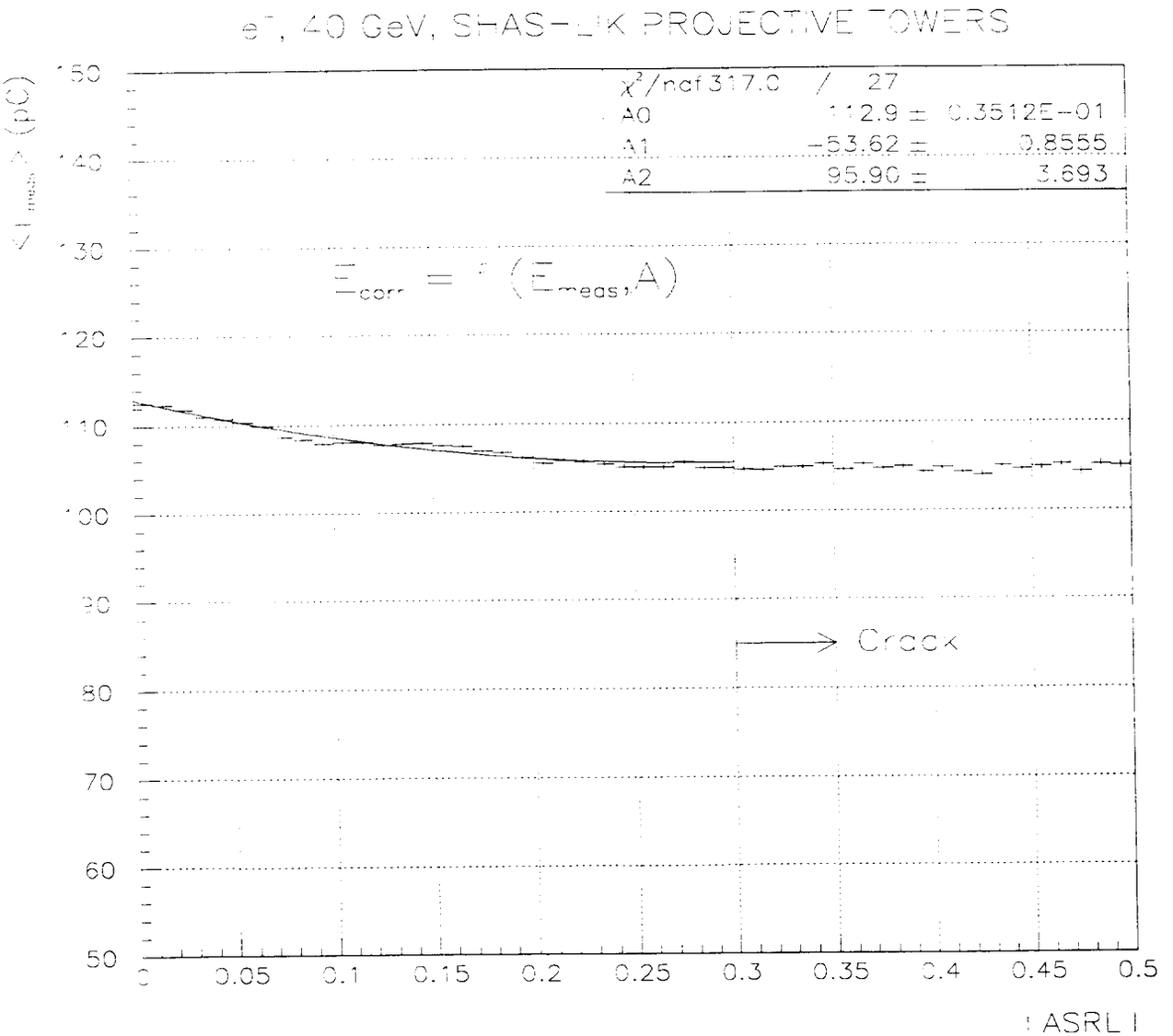

Figure 25: Fitted correction function from mean energy measured vs asymmetry

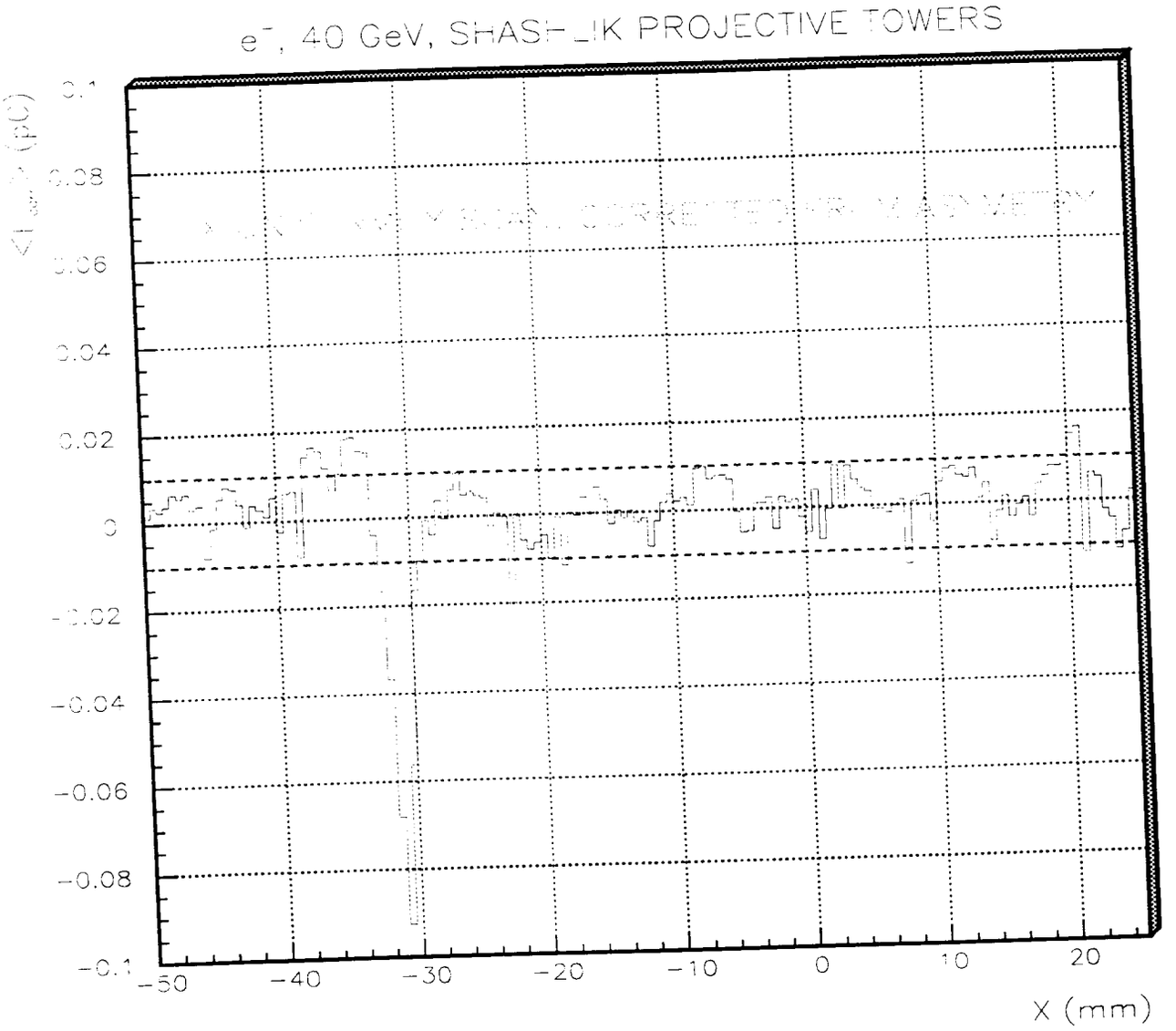

Figure 26: Energy corrected with asymmetry from light collection non-uniformity

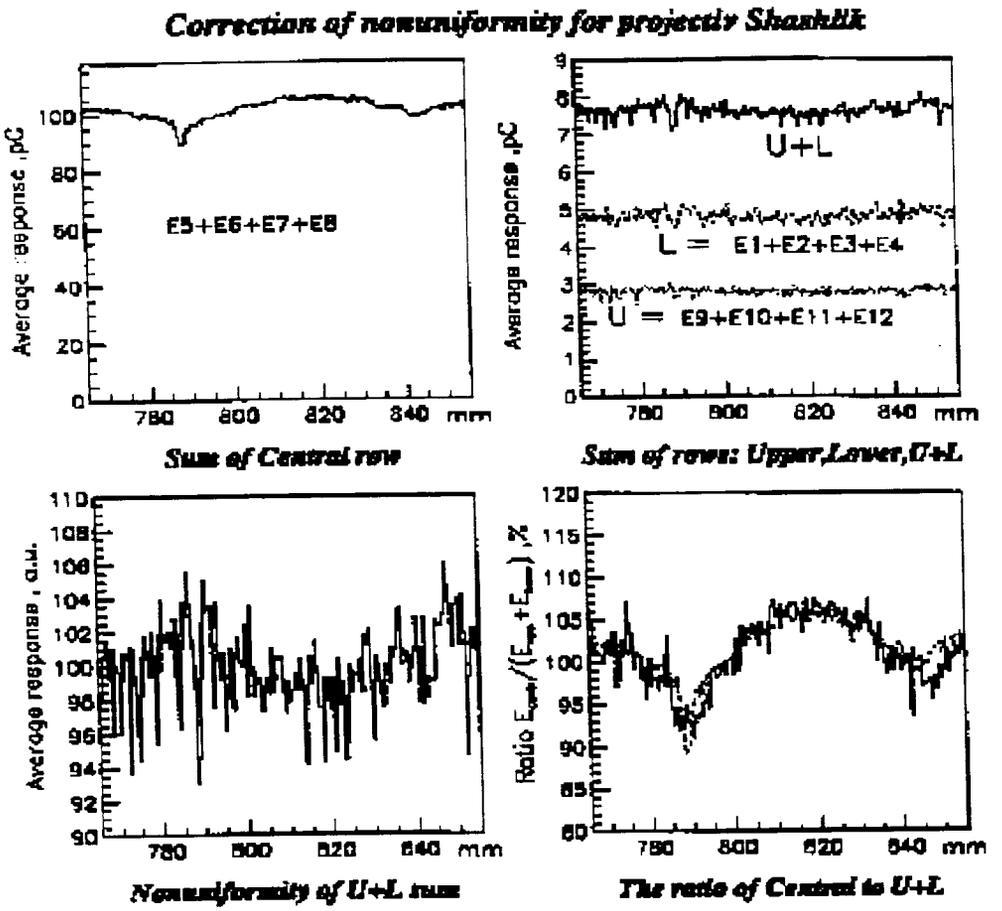

Figure 27: Energy reponse of the central row sum, lower and upper rows sum, and of their ratio for the projective prototype

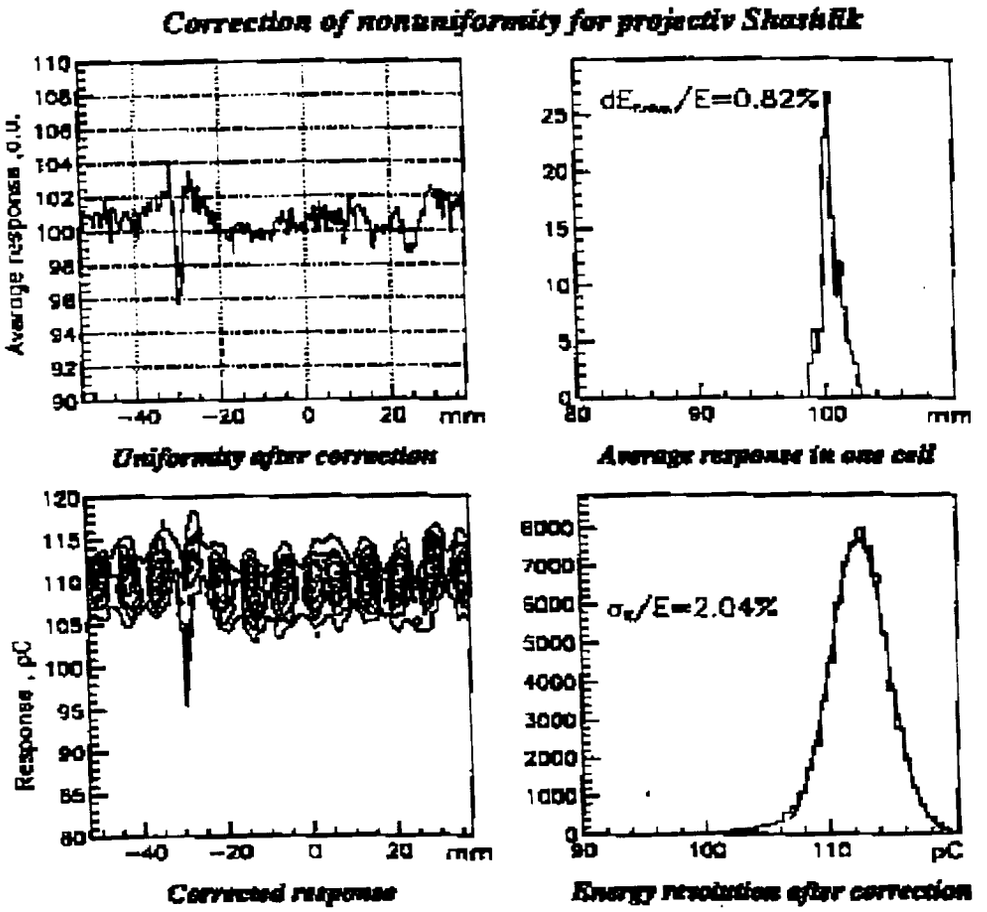

Figure 28: Energy corrected from non-uniformity using the ratio of central to lower and upper rows sum for the projective prototype

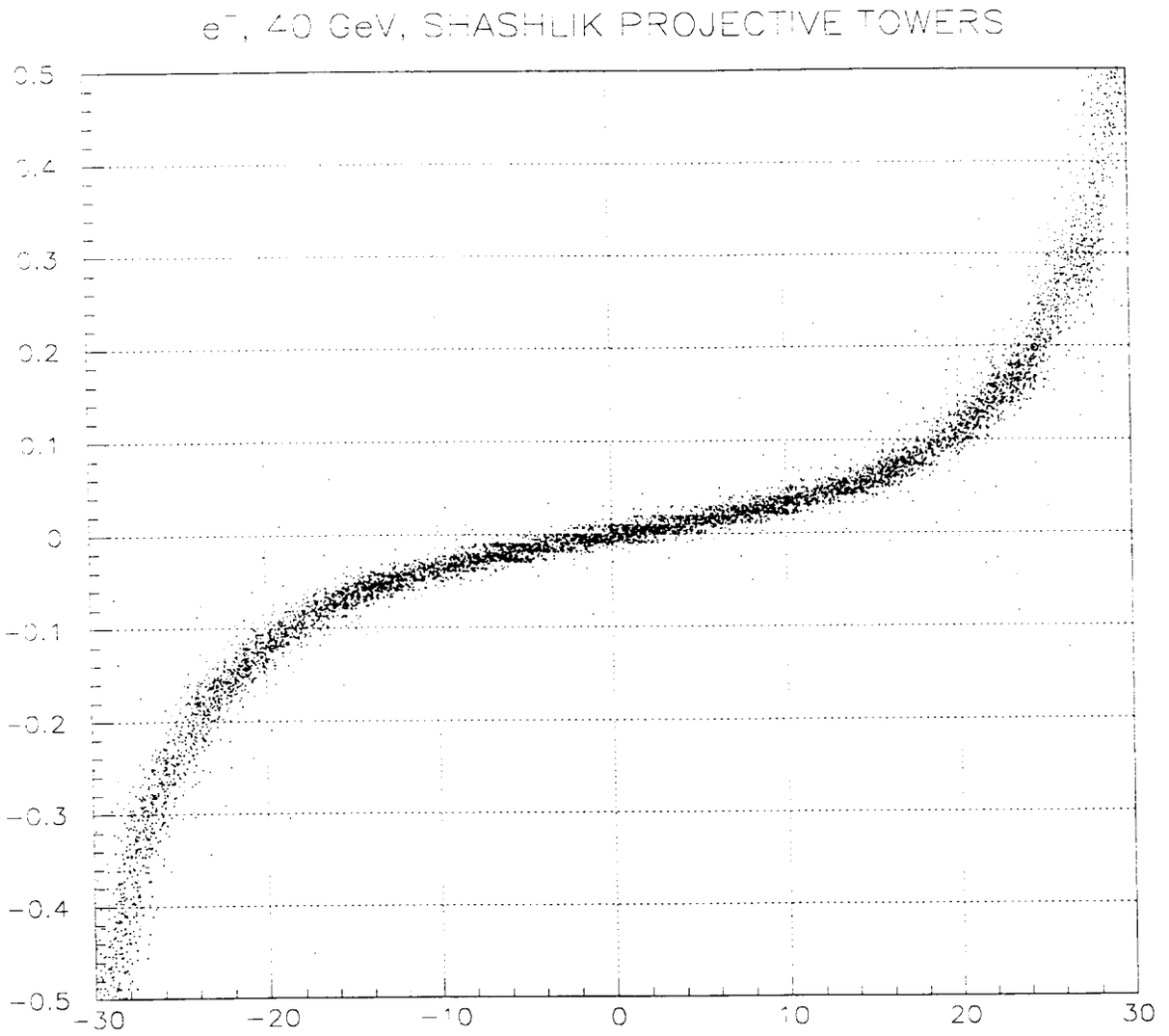

Figure 29: Asymmetry vs beam position for projective prototype and for 40 GeV electrons

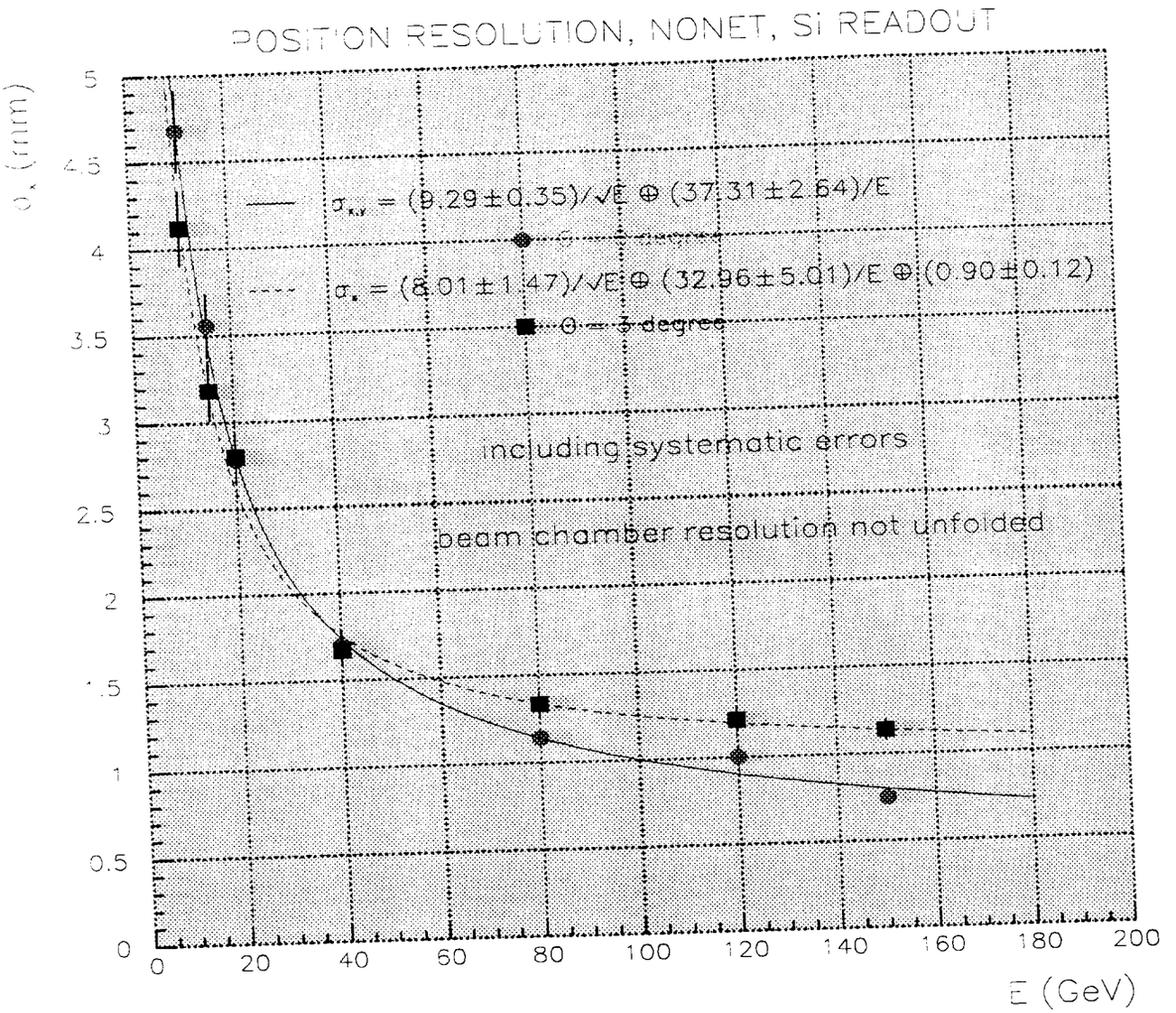

Figure 30: Position resolution for the nonet as a function of beam energy, for $\theta_z = 0$ and for $\theta_z = 3$ degrees

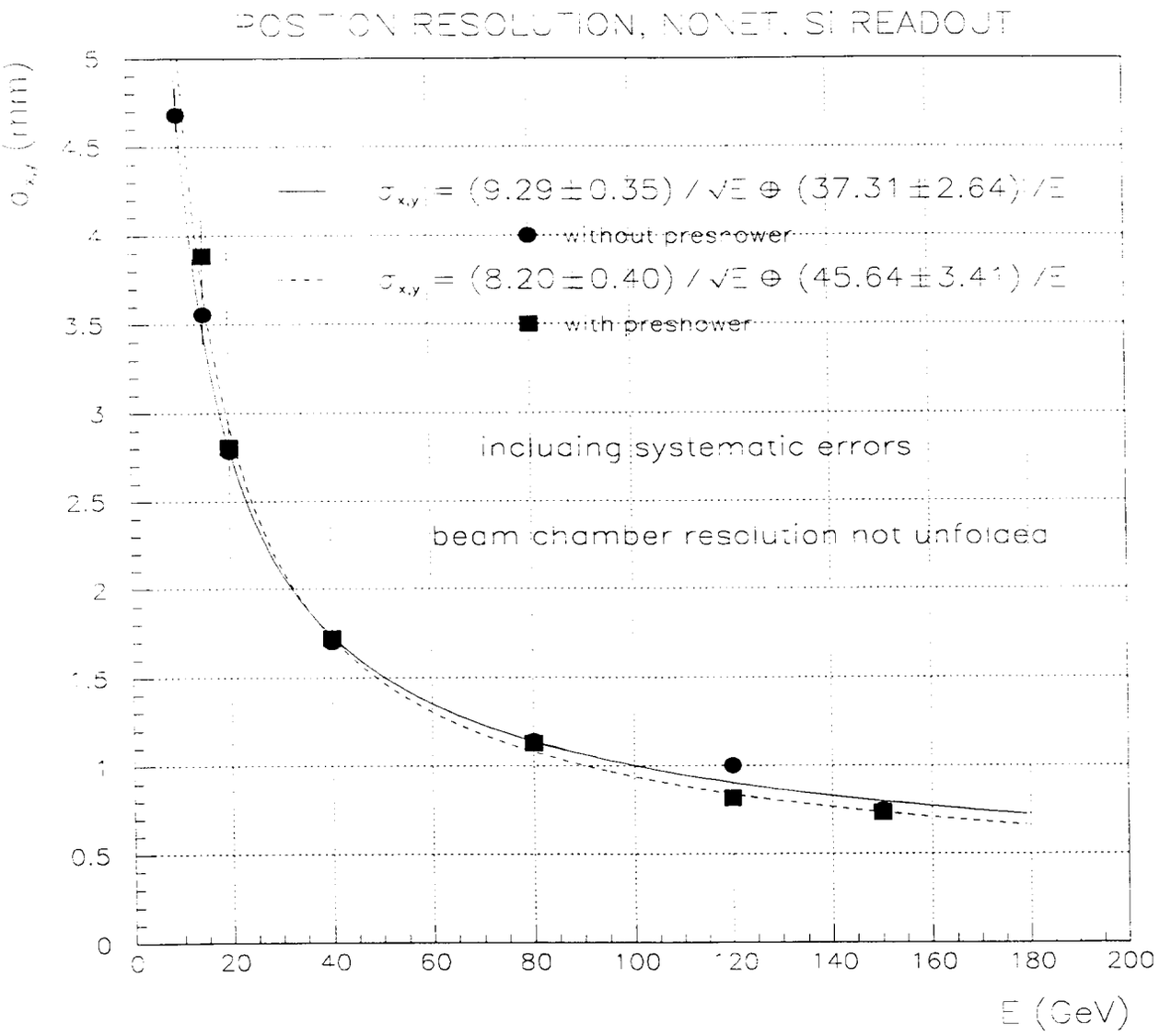

Figure 31: Position resolution for the nonet as a function of the beam energy, without and with preshower in front

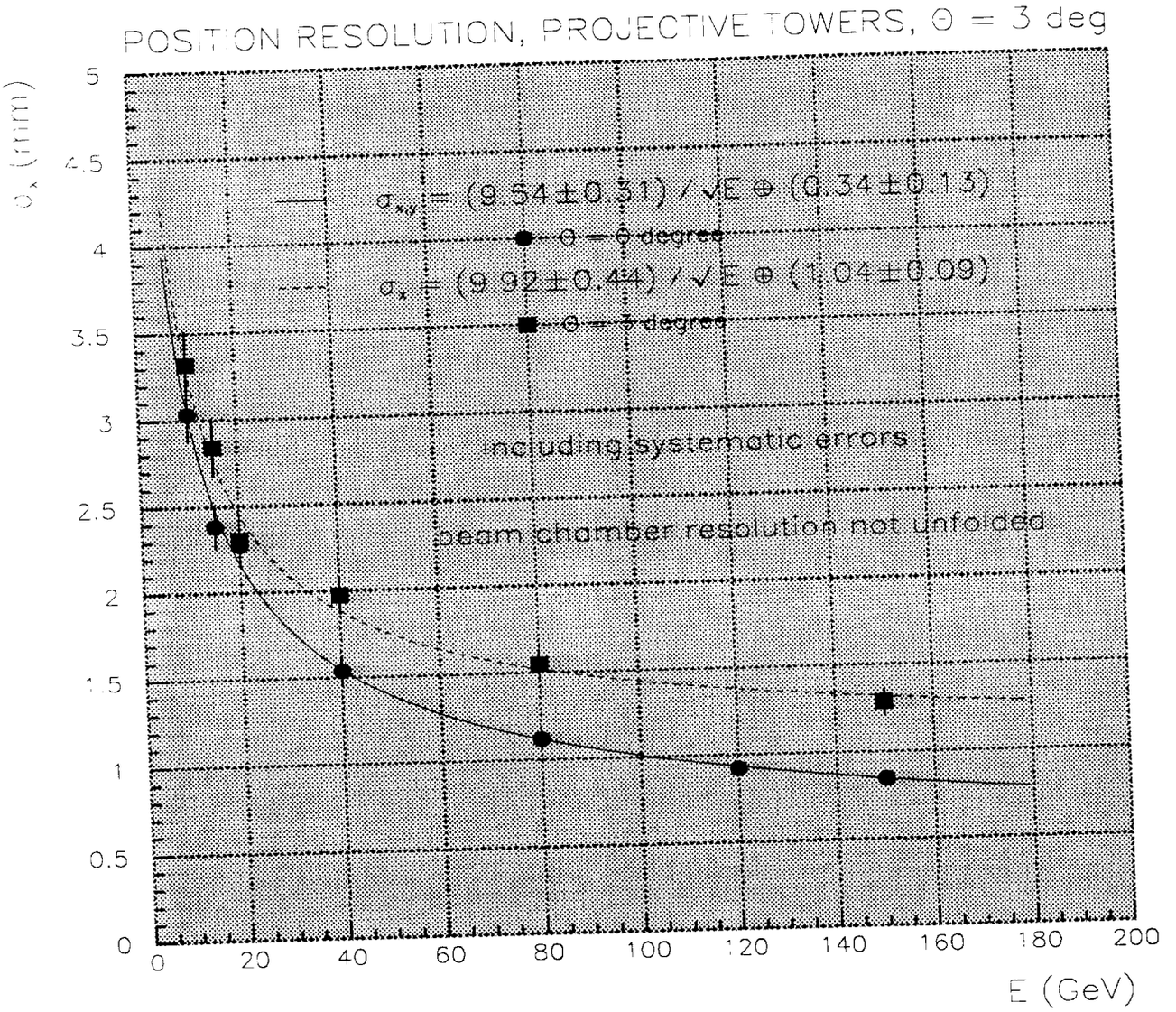

Figure 32: Position resolution for the projective prototype as a function of the beam energy, for $\theta_z = 0$ and for $\theta_z = 3$ degrees

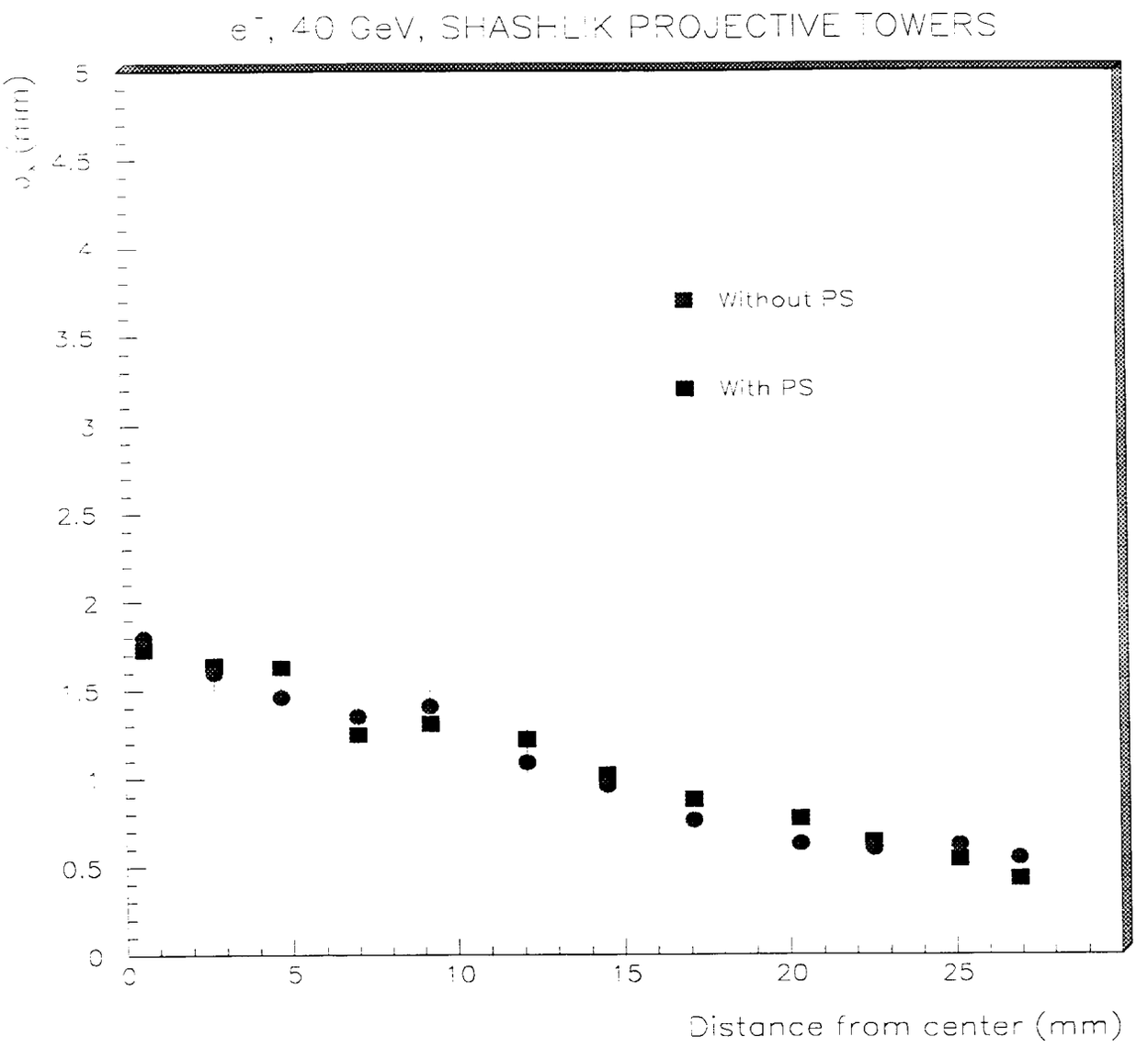

Figure 33: Position resolution for the projective prototype as a function of the distance to the tower center without and with preshower in front

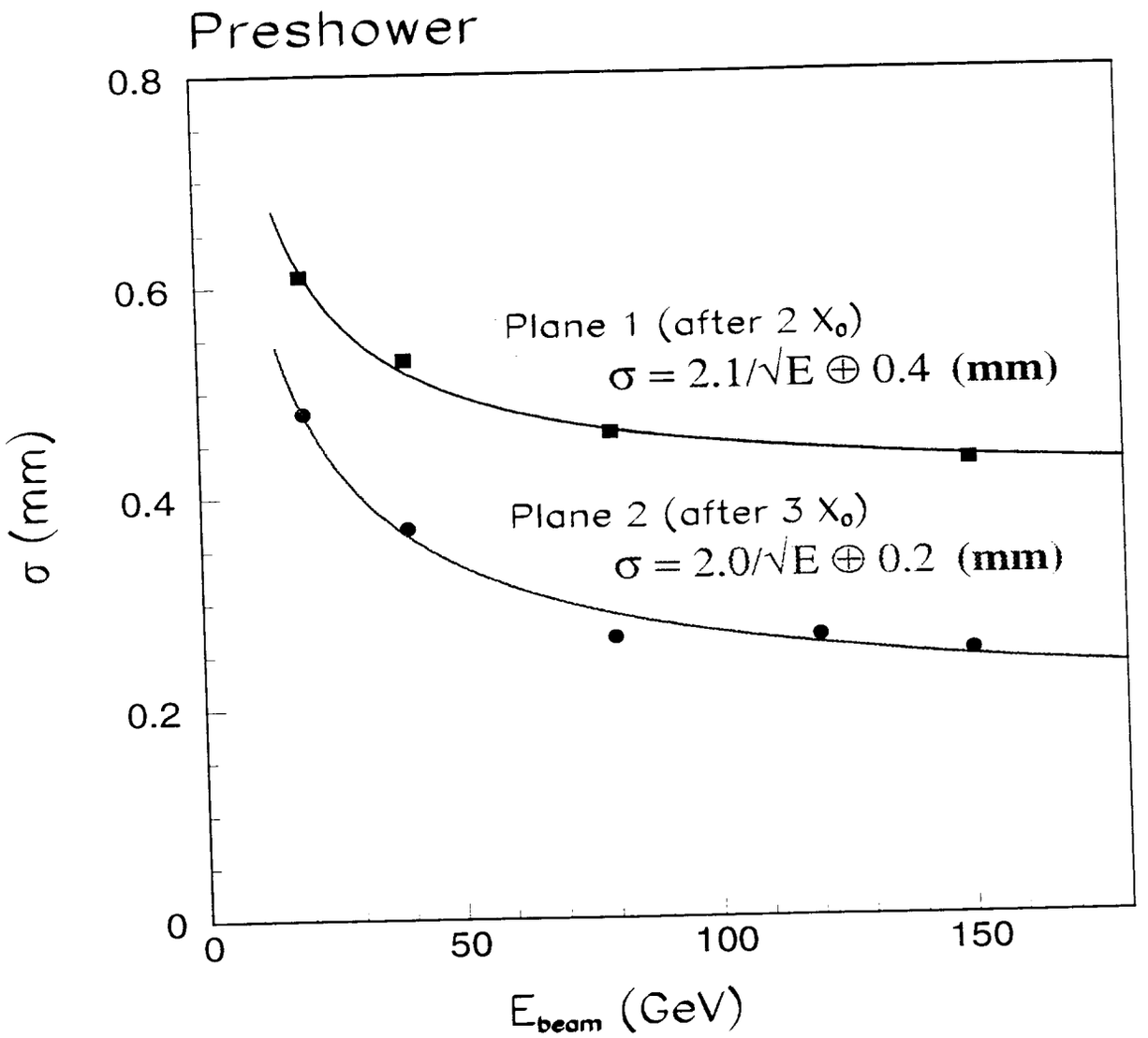

Figure 34: Position resolution for the two preshower planes as a function of the beam energy

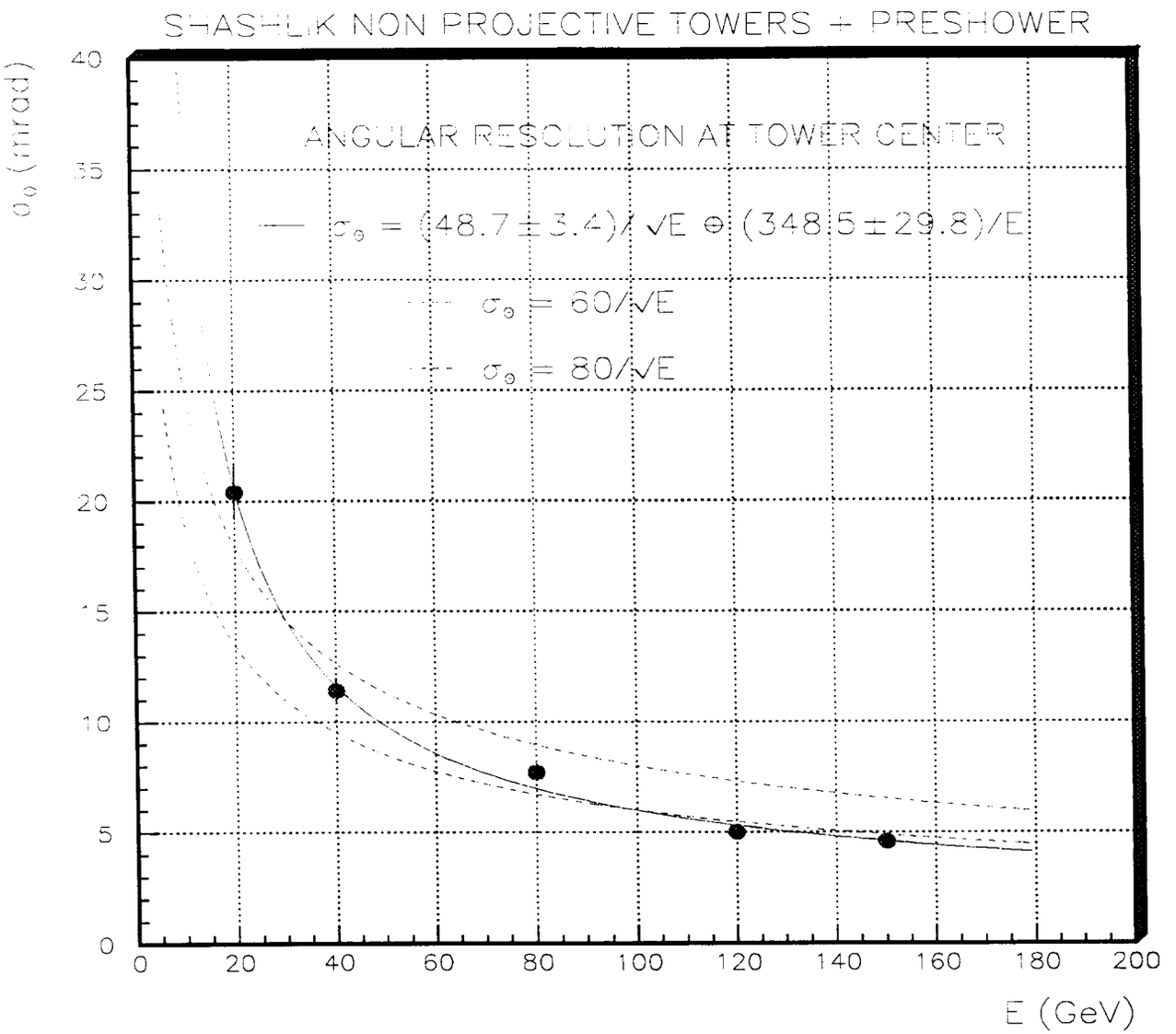

Figure 35: Angular resolution for the projective and preshower combined prototypes as a function of the beam energy and at tower center. The line is a quadratic fit as described in text. Also indicated are the curves corresponding to $\sigma_\theta = \frac{60}{\sqrt{E}}$ and $\sigma_\theta = \frac{80}{\sqrt{E}}$ (dashed lines).

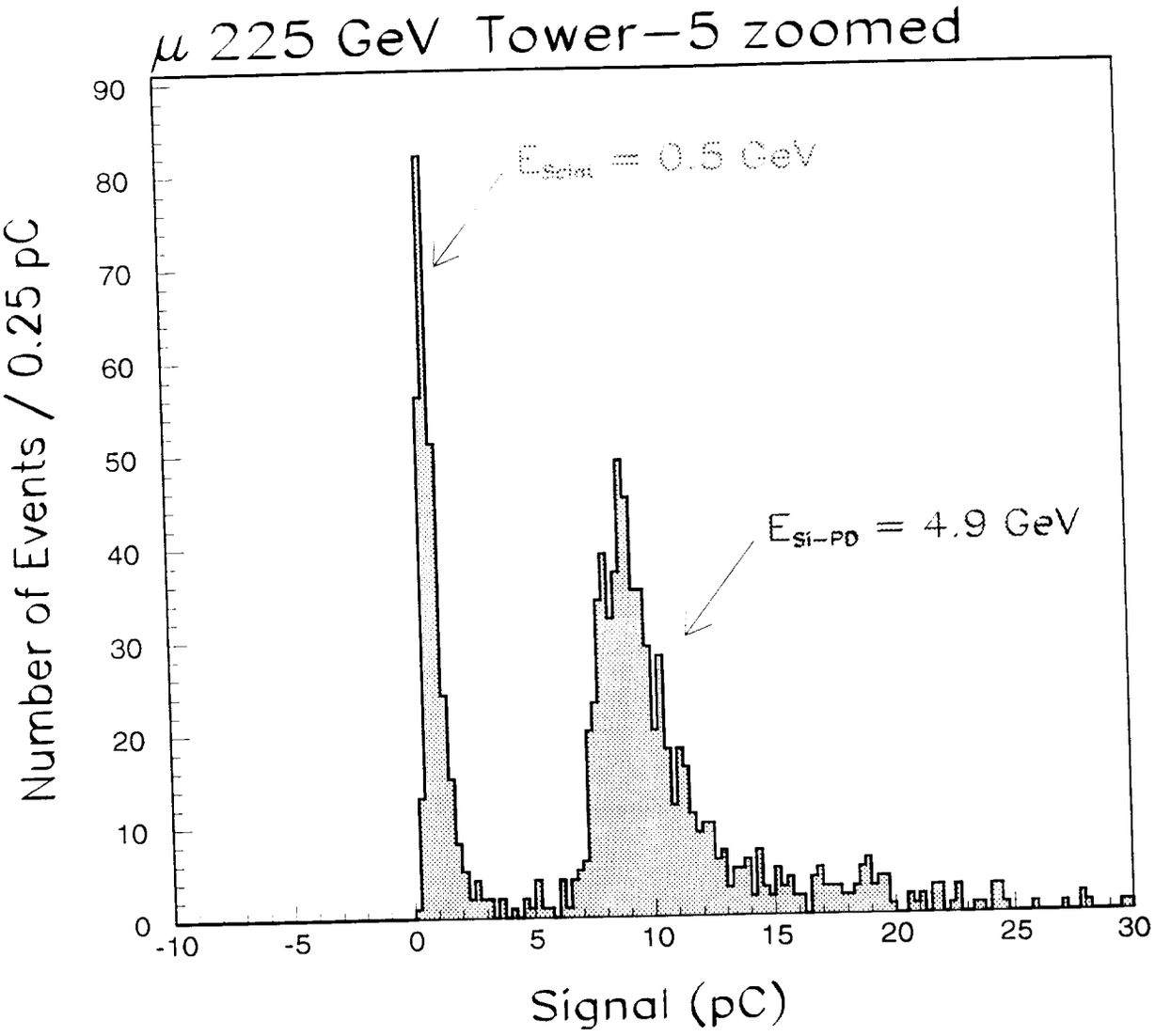

Figure 36: Muon signal distribution with photodiode readout. Vertical scale is arbitrary.

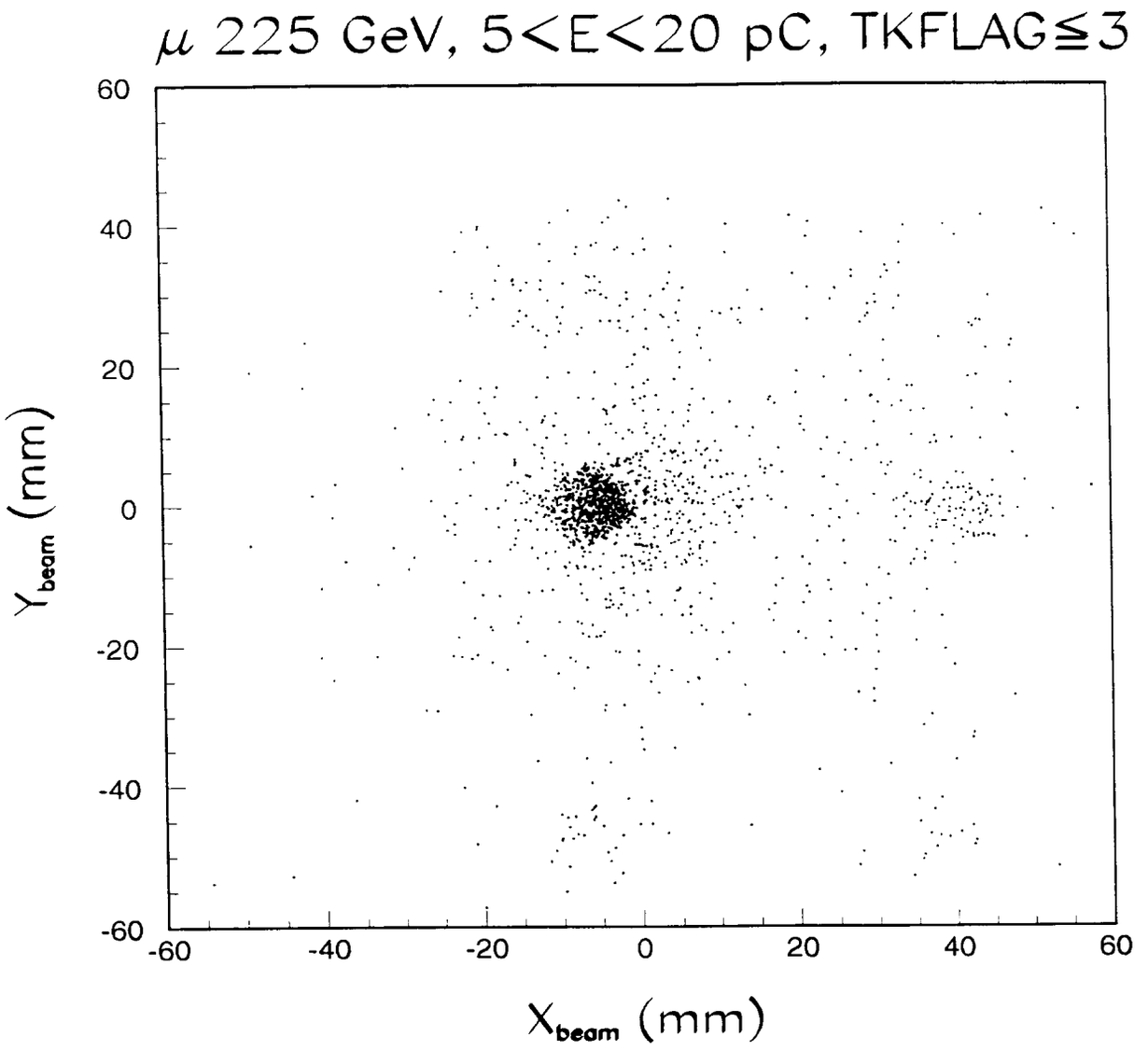

Figure 37: Muon signal as a function of beam coordinates

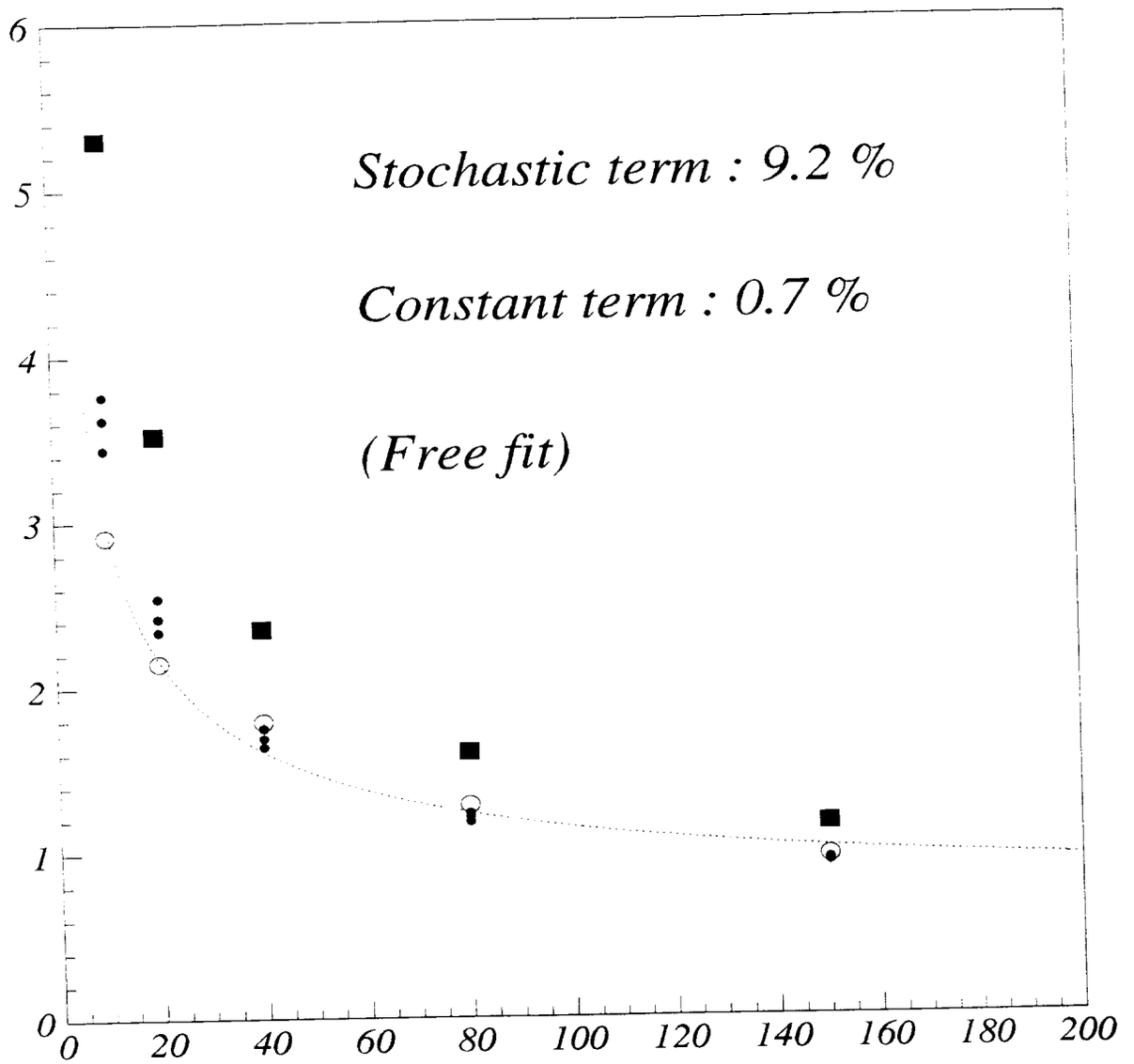

Figure 38: Energy resolution as predicted by Monte Carlo simulation. Empty circles : setup without preshower (fitted). Filled squares : setup with passive preshower. Filled circles : taking into account part/all of preshower information (see text).

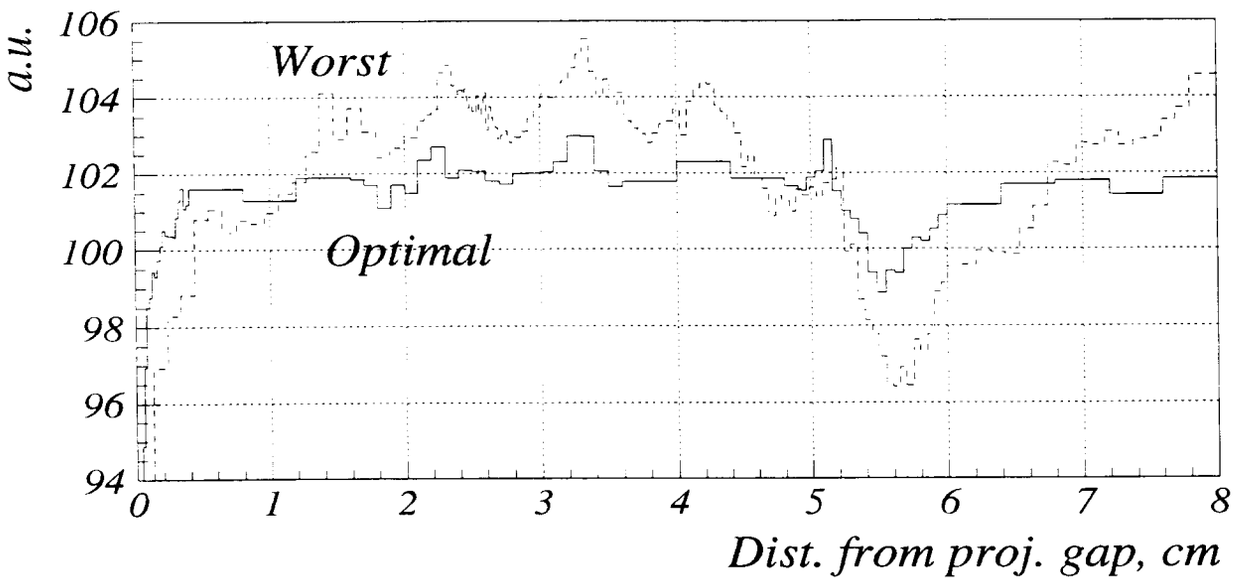

Figure 39: Lateral response, corrected on lateral energy leakage, as predicted by Monte Carlo calculation. Curve marked "Worst" is obtained when using parameters given in section 5.2 in brackets.

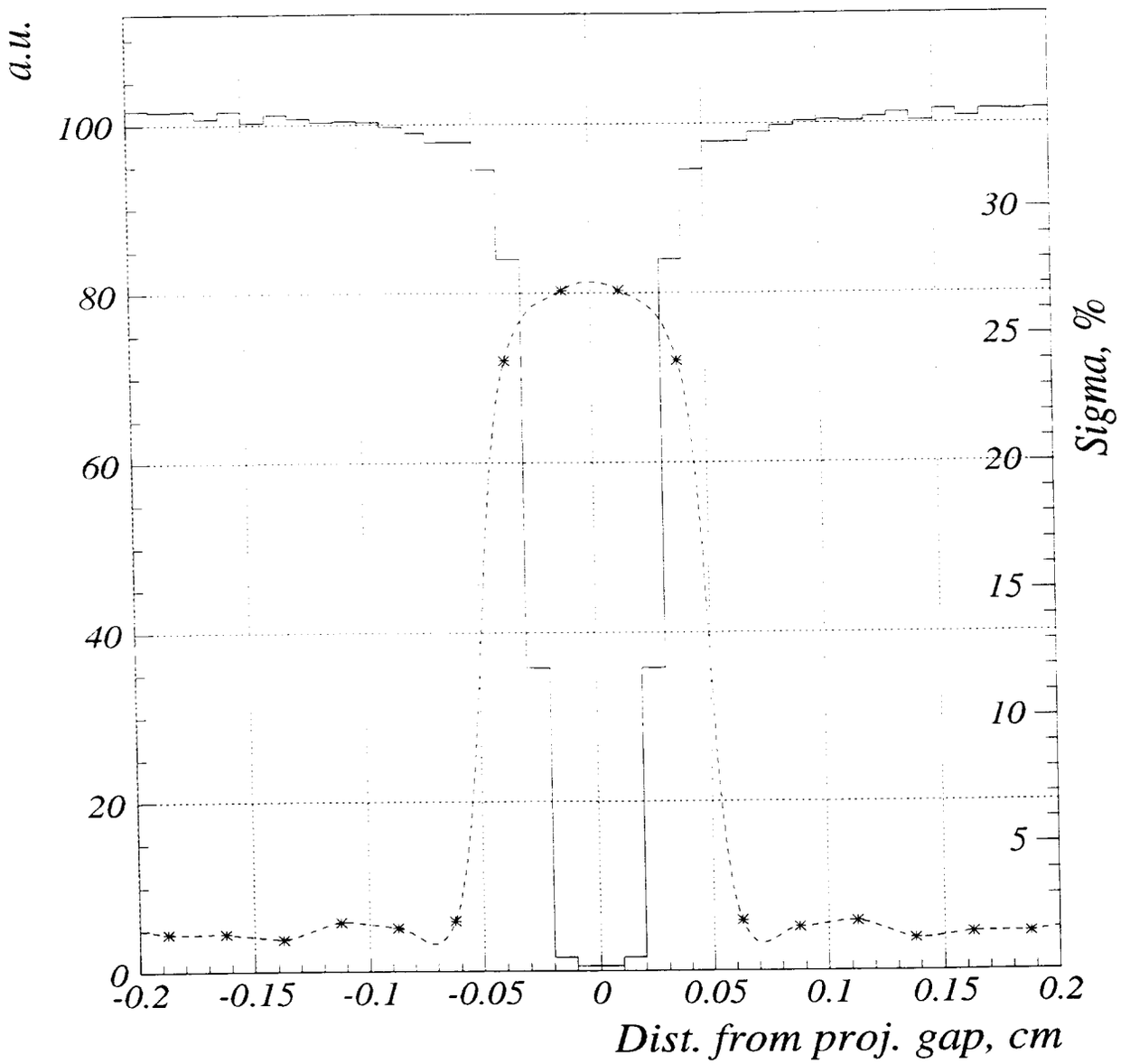

Figure 40: Response in the region of projective gap, as predicted by Monte Carlo. Left axis corresponds to relative average value, and the right axis to sigma (%).

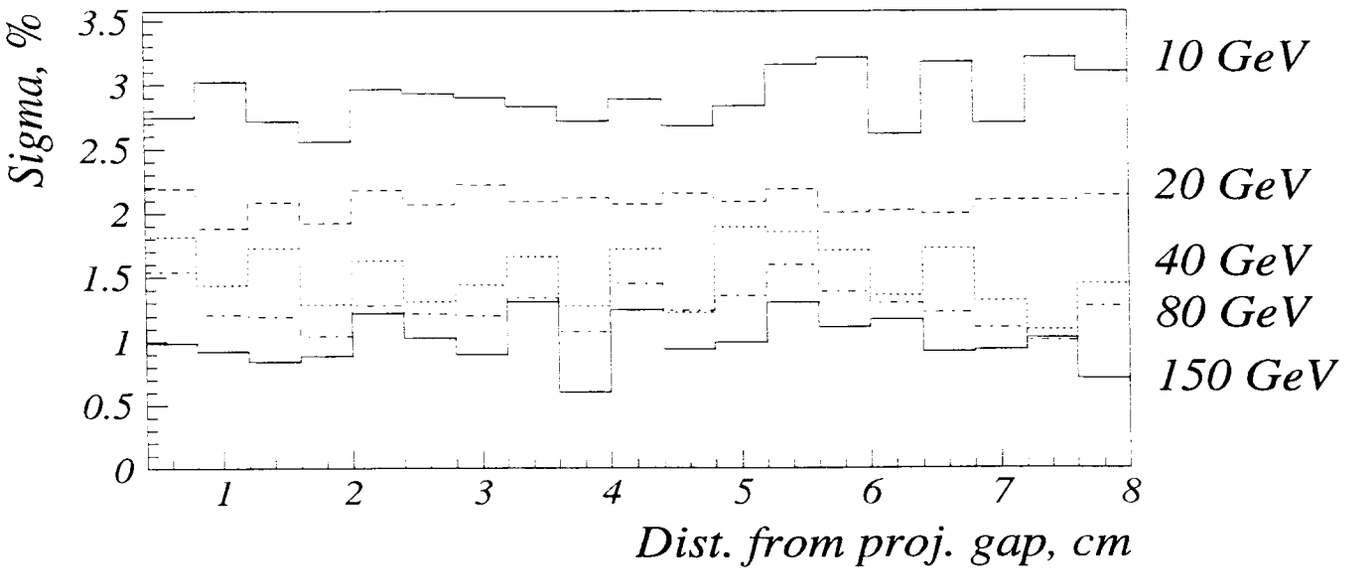

Figure 41: Local energy resolution from Monte Carlo calculation. Five plots correspond to beam energy of 10 to 150 GeV (top to bottom).

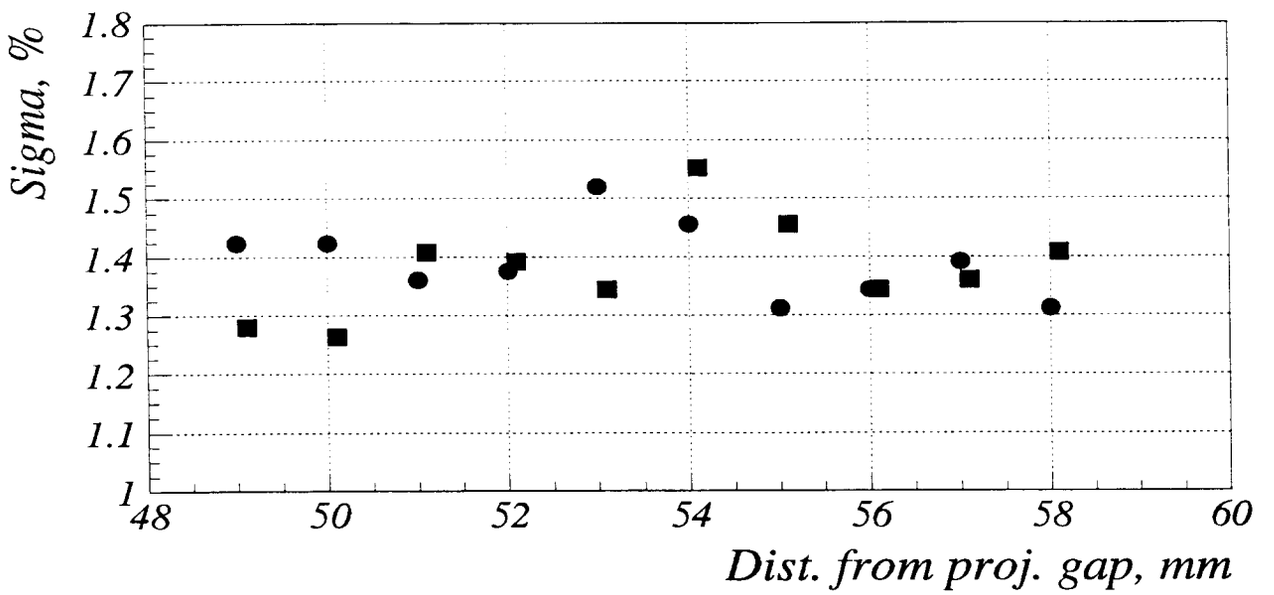

Figure 42: Relative sigma of response for the beam targeted at the points near non-projective gap. Circles : 100 μm of carbon coating of each module, squares : 250 μm. Air gap is 200 μm in both cases.

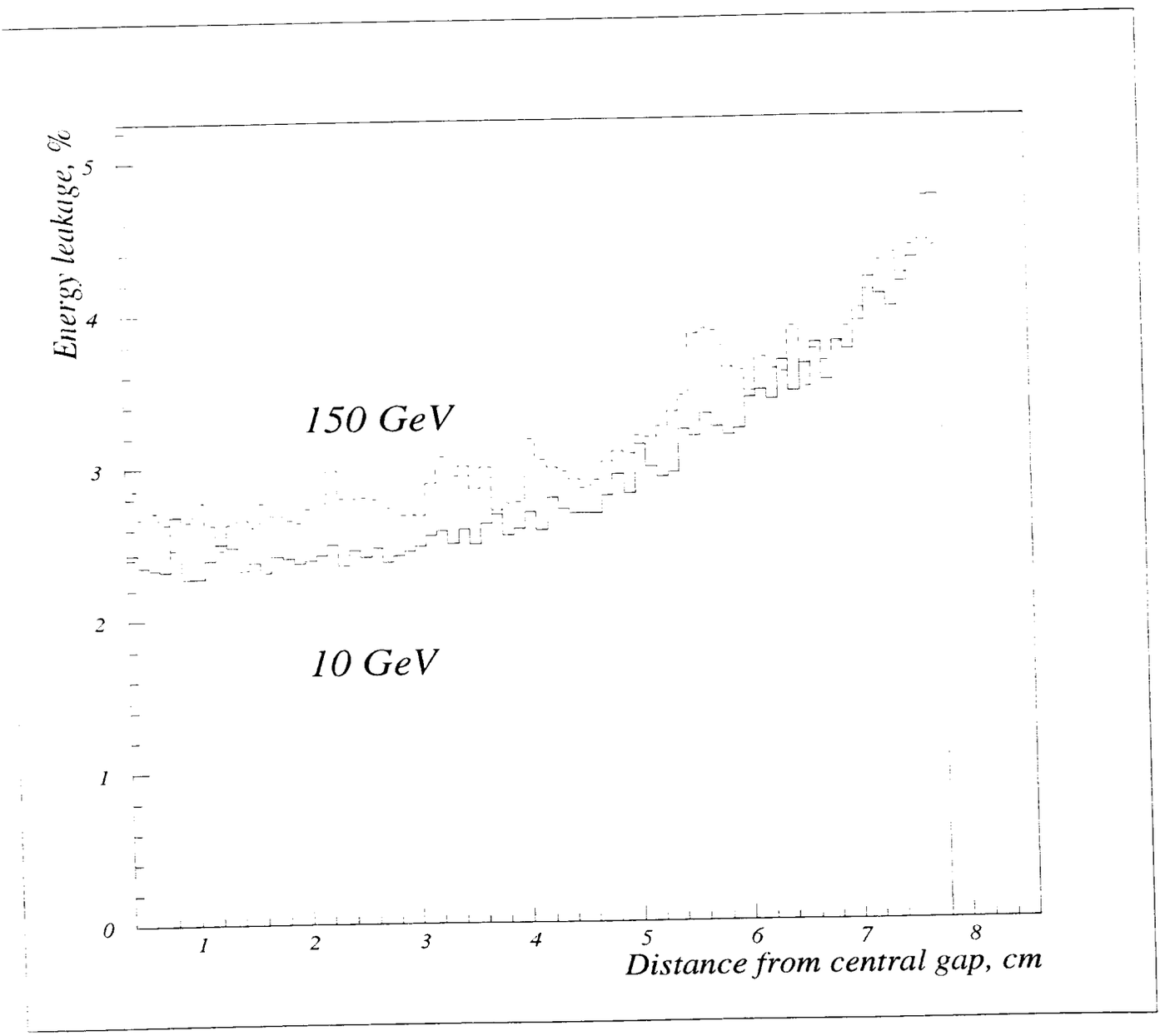

Figure 43: Energy leakage, as predicted from Monte Carlo simulation.

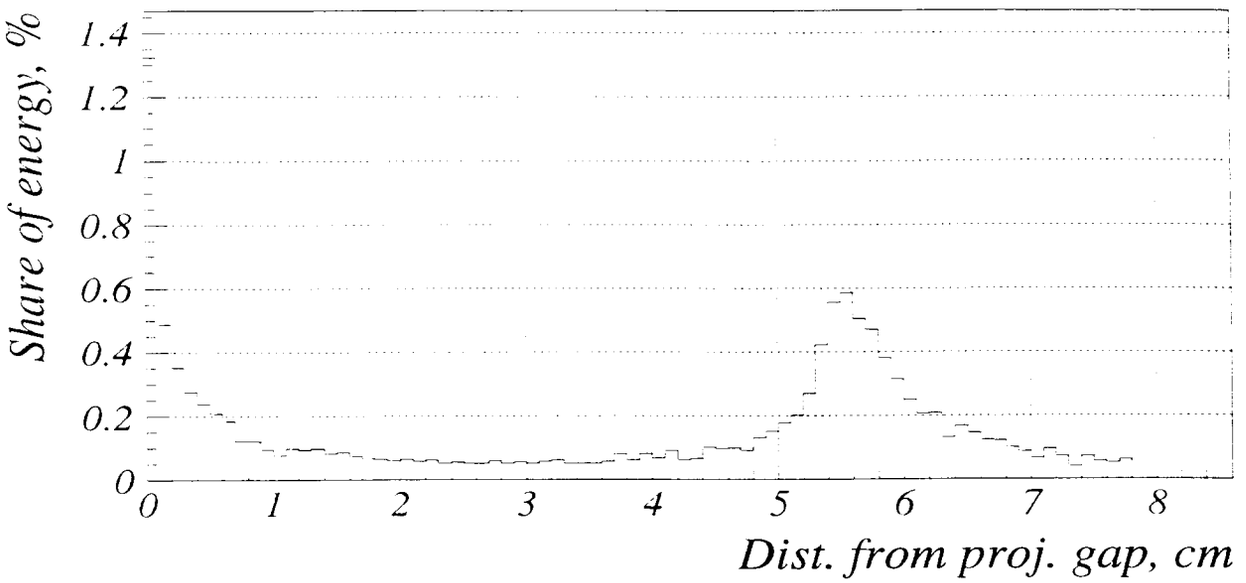

Figure 44: Average values of fraction of energy deposited in projective ends of scintillator tiles for different beam positions, as predicted by Monte Carlo simulation.

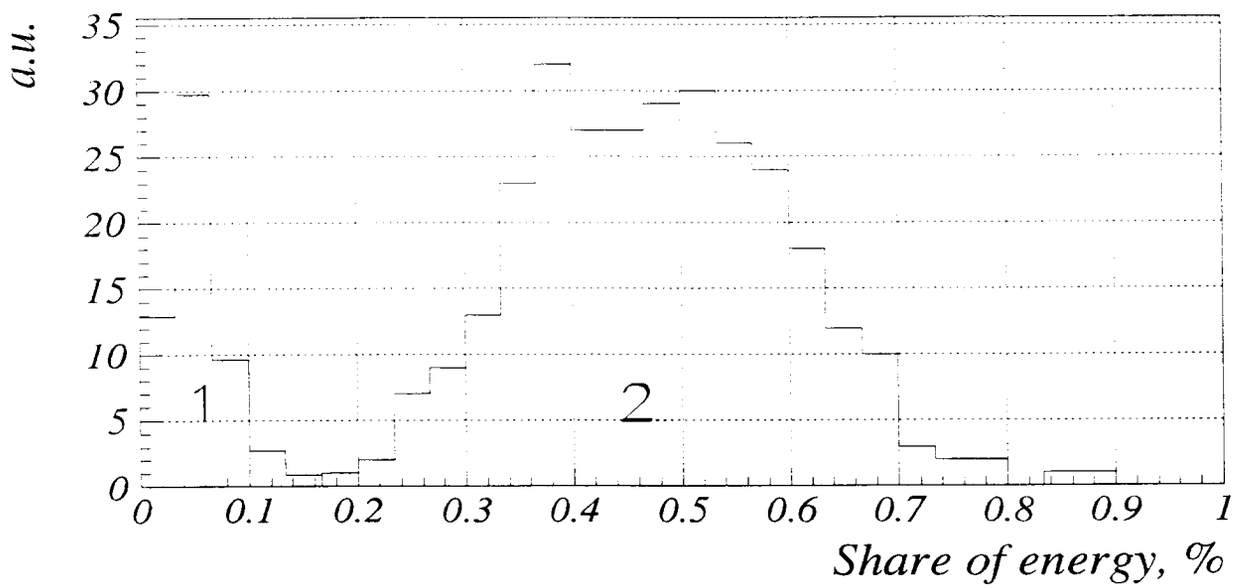

Figure 45: The distributions of the fraction of energy deposited in the projective ends of the scintillator tiles, from Monte Carlo calculation. Plot 1 : beam pointed at the module centre $\pm 3mm$. Plot 2 : at the gap $\pm 3mm$.